DEPARTMENT OF PHYSICS
UNIVERSITY OF JYVÄSKYLÄ
RESEARCH REPORT No. 8/2010

WEAKLY INTERACTING DARK MATTER IN WALKING TECHNICOLOR THEORIES

BY
JUSSI VIRKAJÄRVI

Academic Dissertation
for the Degree of
Doctor of Philosophy

To be presented, by permission of the
Faculty of Mathematics and Natural Sciences
of the University of Jyväskylä,
for public examination in Auditorium FYS-1 of the
University of Jyväskylä on October 8, 2010
at 12 o'clock noon

Jyväskylä, Finland
August 2010

Preface

The work contained in this thesis has been carried out during the years 2006-2010 at the Department of Physics in the University of Jyväskylä.

I wish to thank especially my supervisor Doc. Kimmo Kainulainen for patient guidance and encouragement. His broad knowledge in particle physics and cosmology has given me extensive survey to these fields of physics, and many insights, which have increased both my interest and knowledge in physics during these years. I am also grateful to 'my second supervisor' Doc. Kimmo Tuominen for partial guidance, collaboration and illuminating discussions within the landscape of technicolor. I would also like to thank Prof. Kari Rummukainen and Doc. Iiro Vilja for their valuable comments to this manuscript.

There are also other senior physicists who have shared their knowledge of physics and/or have been a source of inspiration during the course of my studies, from which they will have my gratitude. Mentioning some: Prof. Jukka Maalampi, Prof. Kari Eskola, Prof. emer. Vesa Ruuskanen, Lect. Markku Lehto, Prof. Francesco Sannino, Prof. Kari Enqvist and Prof. emer. Keijo Kajantie.

The collaboration and the discussions spiced with (sometimes peculiar) humor with the co-workers have been both educating and fun. I have enjoyed the atmosphere of the department and for that the thanks do not belong only to the close co-workers but to the whole staff.

I am also grateful for friends and family for their support and interest to my work. I am particularly indebted to my beloved wife Sanna who has always encouraged me to go forward in my chosen path.

The financial support of Finnish Academy of Sciences and Letters; Vilho, Yrjö and Kalle Väisälä foundation, the Academy of Finland; Graduate School of Particle and Nuclear Physics, and the University of Jyväskylä is gratefully acknowledged.

List of publications

This thesis is based on the work contained within the following publications:

I **Weakly interacting dark matter particle of a minimal technicolor theory**
K. Kainulainen, K. Tuominen and J. Virkajarvi,
Phys. Rev. D **75** (2007) 085003, [arXiv:hep-ph/0612247].

II **Weakly interacting dark matter from the minimal walking technicolor**
K. Kainulainen, K. Tuominen and J. Virkajarvi,
JCAP **1002** (2010) 029, [arXiv:0912.2295].

III **Naturality, unification and dark matter**
K. Kainulainen, K. Tuominen and J. Virkajarvi,
Phys. Rev. D **82** (2010) 043511, [arXiv:1001.4936].

Majority of the dark matter calculations in papers I and II and all the dark matter calculations in paper III were carried out by the author. Also all the constraint calculations, except for the electroweak S, T and U parameter analysis, were done by the author. Author also participated to the writing process of the result and constraint sections in papers II and III.

Contents

Chapter 1

Introduction

Several astrophysical observations, including stellar motions in spiral galaxies and galaxy motions in galaxy groups, clusters and superclusters, indicate that there should be much more mass in these systems than what has been optically observed. This apparent presence of non-luminous gravitating mass, is the well-known dark matter problem. These astrophysical observations are further supported by the analysis done from the fluctuations of the cosmic microwave background radiation, which indicates the presence of a dominant non-baryonic matter component in the Universe. According to the present knowledge only $\sim 17\%$ of the total matter density in the Universe is made of normal baryonic matter, while as much as $\sim 83\%$ is dark matter of some unknown origin. Even more enigmatic quantity is the cosmological constant, or dark energy, which sets the expansion of the Universe to accelerate, and which seems to dominate the energy density of the universe, covering $\sim 73\%$ of the total energy density. These dark matter and dark energy problems are among the greatest unsolved mysteries in modern cosmology and physics.

In this thesis the dark matter problem is considered, in the context of a particle dark matter model, embedded in the minimal walking technicolor (MWT) theory. The minimal walking technicolor is a model for the dynamical electroweak symmetry breaking, without a fundamental scalar field, which can be also extended to provide the unification of standard model coupling constants. The pure MWT and its minimal extension, discussed in this thesis, predicts natural particle dark matter candidates such as the fourth family heavy neutrinos and $SU(2)_{\mathrm{weak}}$ adjoint fermions. Specific dark matter models including well defined gauge couplings, effective Higgs couplings, the mass terms and mass mixings and detailed annihilation cross section calculations, accurate relic density calculations and analysis of constraints following from experimental data for the models are represented in papers [I]- [III]. Also the effects of a dynamical dark energy to the dark matter density is studied in paper [I]. It has been demonstrated in these articles that the minimal technicolor dark matter models are plausible and they can produce correct dark matter densities. It is of particular interest that they can be either verified or ruled out by the present

or upcoming dark matter experiments. A more general dark matter model in the MWT context, which combines the models represented in articles [I]- [III], is introduced and studied in some detail in this thesis.

The thesis contains the papers [I]- [III] and an introduction. Introduction contains the part specifying the model and a summary which are organized as follows. The Chapter 2 contains a general discussion of the dark matter from the cosmology point of view, discussion of observations, speculation of the possible nature of the dark matter and the massive cold particle dark matter scenario. The Chapter 3 includes an introduction to technicolor theory and a more specific consideration of minimal walking technicolor model and its extension which predicts the new dark matter particle candidates. In Chapter 4, from these elements a more general dark matter model is constructed. The models and the results presented in articles [I]- [III] can be obtained from this model in certain limits. Also the constrains set by different dark matter search experiments to the general model and limiting cases are discussed in Chapter 4. A global analysis of the general model is yet do be done in the near future.

Chapter 2

Basics of dark matter problem

In this chapter the basic cosmological framework is presented, the main observational and theoretical arguments that support the existence of non-luminous (dark) matter in the universe are introduced and the nature of the dark matter is discussed. Finally the evolution equation for the number density of the massive dark matter particles is derived.

2.1 Cosmological framework

According to observations [1–3] the universe seems to be homogeneous and isotropic at large scales and expanding according to Hubble law[1]. When the observed expansion is viewed backwards, a hot and dense initial state, the big bang, can be conceived to exists at the beginning. The standard cosmological big bang model is, accordingly, built on the *cosmological principle*, that states that the universe at largest scales is homogenic and isotropic. When a universe satisfying the cosmological principle is set to expand the expansion automatically realizes the Hubble law.

The evolution equations of the universe in the big bang model are assumed to follow from the Einsteins field equations (EFE) of the general relativity (GR), which tell how the spacetime metric evolves in the presence of matter and energy. The matter and energy content of the universe which form the source in the field equations need to be chosen to follow the observed symmetries which implies that also the corresponding metric needs to respect the cosmological principle. The metric that fulfills these symmetry arguments is called Friedmann-Lemitre-Robertson-Walker (FLRW) metric which can be written as

$$\mathrm{d}s^2 = g_{\mu\nu}\mathrm{d}x^\mu \mathrm{d}x^\nu = \mathrm{d}t^2 - a^2(t)\left(\frac{\mathrm{d}r^2}{1-kr^2} + r^2\mathrm{d}\theta^2 + r^2\sin^2\theta\mathrm{d}\phi^2\right), \qquad (2.1)$$

[1]The expansion of the universe was first discovered by Edwin Hubble in late 1920's. He observed that the velocities of distant galaxies increase linearly as a function of their distance and derived the Hubble law: $v = H_0 r$, where $H_0 = 100\,h\,\mathrm{km\,s^{-1}\,Mpc^{-1}}$ with $h = 0.73(3)$ [4] is the present measured value for the Hubble constant.

where t, r, θ, ϕ are the co-moving time and spherical coordinates respectively and $a(t)$ is the time dependent *scale factor* that describes the evolution of the physical distances in the universe, or loosely speaking the size of the universe. Finally k specifies the geometry of the space-time so that for $k = 0, +1 \text{or} -1$ the universe is flat, closed or open respectively.

Einsteins field equations of the general relativity follow from the principle of least action for $S = S_{\text{E}-\text{H}} + S_{\text{SM}}$, where the Einstein-Hilbert action $S_{\text{E}-\text{H}}$ and matter action the S_{SM} are defined as

$$S_{\text{E}-\text{H}} = -\frac{1}{16\pi G_N} \int \mathrm{d}^4x\sqrt{-g}(R + 2\Lambda), \tag{2.2}$$

$$S_{\text{SM}} = \sum_i^{\text{fields}} \int \mathrm{d}^4x\sqrt{-g}\mathcal{L}_i. \tag{2.3}$$

Here g is the determinant of the metric tensor $g_{\mu\nu}$, R is the Ricci scalar, Λ is the cosmological constant and the S_{SM} contains the sum of Lagrangian densities $\mathcal{L}_i$ for all the matter and gauge fields belonging to the standard model (SM) of particle physics or its possible extensions. When the functional variation for the S is taken with respect to the metric tensor $g_{\mu\nu}$ the Einsteins field equations of the general relativity follow:

$$R_{\mu\nu} - \frac{1}{2}g_{\mu\nu}R - \Lambda g_{\mu\nu} = 8\pi G_N T_{\mu\nu}, \tag{2.4}$$

where $R_{\mu\nu}$ is the Ricci tensor and the energy momentum tensor is defined as $\sqrt{-g}T_{\mu\nu} = -2\delta S_{\text{SM}}/\delta g^{\mu\nu}$.

In the standard cosmological model the matter and energy content of the universe is described by the energy momentum tensor of the perfect fluid form;

$$T_{\mu\nu} = (p + \rho)u_\mu u_\nu - p g_{\mu\nu}, \tag{2.5}$$

where p, ρ and u^μ are the pressure, the energy density and the four velocity of the fluid respectively. The different fluid components respect the equation of state $p = \omega\rho$, where $\omega = 0$ for matter (dust), $\omega = 1/3$ for radiation and $\omega = -1$ for cosmological constant. Furthermore $\omega = \omega(t)$ is possible for exotic fluids modeling a dynamical dark energy[2].

When the FLRW metric Eq. (2.1) is substituted to the Einstein field equations Eq. (2.4) simplify dramatically because of the symmetry; only non-trivial components are the 00 and 11 (all ii-components are the same, in fact) which are called the Friedmann equations:

$$\left(\frac{\dot{a}}{a}\right)^2 + \frac{k}{a^2} = \frac{8\pi G_N}{3}\rho_{tot}, \tag{2.6}$$

[2]Note that $\omega_{tot} = p_{tot}/\rho_{tot}$ generally depends on t even without exotic fluids if system contains different fluids.

$$2\frac{\ddot{a}}{a} + \left(\frac{\dot{a}}{a}\right)^2 + \frac{k}{a^2} = -8\pi G_N\, p_{tot}. \tag{2.7}$$

Here dot denotes the time derivative, and the total energy density and the total pressure are defined as $\rho_{tot} = \rho_{rad} + \rho_{mat} + \rho_\Lambda$ with $\rho_\Lambda \equiv \Lambda/(8\pi G_N)$ and $p_{tot} = p_{rad} + p_{mat} + p_\Lambda$ with $p_\Lambda = -\rho_\Lambda$ for a cosmological constant. Friedmann equations for the evolution of the scale factor are the basis of the standard big bang cosmology. The first Friedmann equation, Eq. (2.6) describes the expansion of the universe and the second, Eq. (2.7) its acceleration. Further, from the covariance of the Einsteins equations it follows that the covariant derivative of the energy momentum tensor vanishes i.e. $T^{\mu\nu}_{;\nu} = 0$, which guarantees the conservation of the energy and the momentum of the fluid. With the help of Eq. (2.6) this can be written in a continuity equation

$$\dot{\rho} = -3H(\rho + p), \tag{2.8}$$

where $H \equiv \dot{a}/a$ is the Hubble expansion parameter. The different scaling laws for energy densities can be derived by using the continuity equation and the equation of state of the fluid ω_i resulting generally (for non-interacting fluids) to

$$\rho_i \propto a^{-3(1+\omega_i)}\,, \tag{2.9}$$

from which the scalings for different fluids follow; for matter (dust) $\rho_m \propto a^{-3}$, for radiation $\rho_{rad} \propto a^{-4}$ and for cosmological constant naturally $\rho_\Lambda \propto$ const.

The evolution of the universe is completely determined by the energy (and pressure) content of the universe. Note that normal matter naturally decelerates the expansion of the universe since it is gravitationally attractive. However fluids with an equation of state $\omega < -1/3$ tend to accelerate the expansion. This is the case for example for the cosmological constant. Defining the critical density $\rho_c \equiv 3H^2/(8\pi G_N)$ and the conventional dimensionless density parameters:

$$\Omega_m \equiv \frac{\rho_m}{\rho_c}\,, \quad \Omega_{rad} \equiv \frac{\rho_{rad}}{\rho_c}\,, \quad \Omega_\Lambda \equiv \frac{\Lambda}{3H^2} = \frac{\rho_\Lambda}{\rho_c} \text{ and } \Omega_K \equiv \frac{-k}{a^2H^2}\,, \tag{2.10}$$

the first Friedman equation Eq. (2.6) can be recast in form

$$\Omega_m + \Omega_{rad} + \Omega_\Lambda + \Omega_K = 1\,. \tag{2.11}$$

By measuring the density parameters (Ω) today, with the Hubble expansion rate, the evolution and age of the universe can be derived. This can be seen from the first Friedman equation Eq. (2.6) when it is written, with the help of Eqs. (2.9) and (2.10), in a more transparent form

$$H = H_0 \left[\Omega_{m,0}\left(\frac{a_0}{a}\right)^3 + \Omega_{rad,0}\left(\frac{a_0}{a}\right)^4 + \Omega_{\Lambda,0} + \Omega_{K,0}\left(\frac{a_0}{a}\right)^2\right]^{1/2}, \tag{2.12}$$

where now the index 0 refers to the present value. Thus determining the present values of density parameters and Hubble parameter with high accuracy is one

of the main goals in modern cosmology. (For more on basic cosmology see e.g. [5, 6].)

A generic, although more speculative part of the standard cosmological model is the cosmic *inflation* (see e.g. review [7]), a short period of time in which universe expands exponentially. Inflation can be described by Friedmann equations consistent with the general relativity. It is expected to happen at very early times right after the big bang and it is usually modeled by dynamical inflation field(s). There are several theoretical and observational motivations for introducing inflation. These include the overall smoothness of and the apparently acausal structures seen in the *cosmic microwave background* (CMB) radiation and the flatness of the universe. Inflation stretches the spacetime exponentially which explains how apparently causally disconnected parts of the universe seen in the CMB actually can belong to a single causally connected region prior inflation. Similarly, the exponential growth of the scale factor forces the observed universe to seem extremely flat, irrespective of its original curvature. Further, and most importantly, the quantum fluctuations during inflation have been shown to be able to create the seeds of structures seen in the universe; the natural prediction of the inflation of the nearly scale invariant spectrum is consistent with the observations. Also the absence of magnetic monopoles and other unwanted topological relics can be explained with inflation which may drive the densities all of these relics toward zero during the exponential expansion. Yet the SM particle content is expected to be created after the inflation in the *reheating/preheating* when the inflation field dumps its energy into SM matter fields.

Now, assuming that the universe is flat as a consequence of the inflation i.e. $\Omega_K = 0$, and since the radiation density is negligible in the present universe, the total energy density is expected to be dominated, and thus the evolution of the universe to be determined, by the matter density and the cosmological constant, whereby the Eq. (2.11) reduces to $\Omega_m + \Omega_\Lambda = 1$. The most successful cosmological model, the ΛCDM model containing a cosmological constant Λ and an exotic dark matter component in addition to ordinary matter is just of this form. The ΛCDM model fits very well to the CMB radiation data, collected by the Wilkinson Microwave Anisotropy Probe (WMAP) satellite and other CMB-observations, producing the inferred values $\Omega_m \approx 0.27$, $\Omega_\Lambda \approx 0.73$ and $\Omega_{tot} \approx 1$. These values are supported by the Hubble Space Telescope data on H_0 and by the observations of Baryonic Aqoustic Oscillations (BAO) in the large scale structure of galaxy distribution [8]. Thus the cosmological constant appears to dominate the energy density and the expansion of the universe seems to be accelerating. Of course the question of the origin and existence of dark energy is still unknown and debated. However in the end the main interest in this work is on the matter density and its decomposition.

In the ΛCDM model the pressureless matter density further decomposes such that the density parameter for baryons is $\Omega_b \approx 0.046$ [8] and, since there is no observations of any other luminous matter, the difference $\Omega_{DM} \approx 0.23$ [8] is associated with some non-luminous dark matter of unknown origin.

It should also be noted that the *Big Bang nucleosynthesis* (BBN) [9] explains very well the observed fractional abundances of light elements: hydrogen, deuterium, helium, and lithium. (The heavier elements are mainly produced in stars and released to the space in supernova explosions.) The BBN predictions for the abundances of the light elements can be calculated as a function of the baryon-photon ratio, and thus when the observed light element abundances are compared to BBN predictions, the present baryon-photon ratio can be determined. From these considerations the baryon density parameter can be solved, resulting in $\Omega_b \approx 0.04$ [9], in a nice agreement with the WMAP results.

Thus both the BBN and the CMB results agree in that baryons cannot explain the whole matter content of the universe, even if non-luminous. Other evidence for existence of dark matter also exist. These questions, as well as the issues concerning the nature of the dark matter, will be considered in more detail in next section. Before that a few words will be spent discussing the dominant dark energy component in the Universe.

Dark energy and Quintessence

According to the ΛCDM model the cosmological constant dominates the present energy density of the universe. Yet the origin and the smallness of its value are unsolved problems. The first assumption could be that Λ is the vacuum energy predicted by quantum field theories. However the value of the observed constant is $\rho_{\Lambda,0} = 0.73\rho_{c,0} \sim (10^{-3}\text{eV})^4$ while a generic field theory prediction is $\rho_{QFT} \sim (\Lambda_{UV})^4 \sim (10^{19}\text{GeV})^4$. Clearly the difference is so huge that quantum fluctuations cannot be attributed to the cosmological constant at least without some extremely delicate and unknown mechanism of fine-tuning. Another puzzle concerns the question why the cosmological constant has started to dominate the energy density only recently. Because the energy density of matter scales as a^{-3} the energy density ratio which today is $\Omega_{\Lambda,0}/\Omega_{m,0} \approx 2.7$ was, for example at the time of recombination $\Omega_{\Lambda,0}/(\Omega_{m,0}(1+z_{\text{rec}})^3) \approx 2.7 \times 10^{-9}$. Thus the fact that right now, when we are observing the universe, the ratio is of the order of one seems fortuitous. It would be much more sensible if there was some natural explanation for the smallness of the dark energy component so that the observed density ratio would not be just a result of some unnatural fine-tuning.

In summary, although the cosmological constant fits best the observations, it is worth considering whether the cosmological constant is really a constant or rather something else which at late times appears as an effective cosmological constant. On boarder sense the question is whether there are any other possible explanations for the cosmic acceleration[3] than the cosmological constant? Several different scenarios have been considered.

One recently studied option is to drop the cosmological principle at the late times in the evolution of the universe, while still keeping the GR as correct theory

[3]See e.g. a short review about cosmic acceleration and dark energy [10].

of gravity. The idea is that the inhomogeneities and the non-linear corrections to the Einstein equations could alter the properties of light, mimicking the effect of a cosmological constant. (See for example [11].)

Another option is to change the GR for example by replacing the Ricci scalar in Einstein-Hilbert action with some more general function f(R). However the constrains coming from solar system dynamics appear to minimize the allowed corrections to GR so that these models can deviate only very little from the GR with a cosmological constant [12].

Another class of models include some exotic fluids which manifest themselves as a dynamical dark energy with an equation of state $\omega_Q(t)$ with a present value $\omega_Q(t_0) \approx -1$. Although the origin and the specific nature of the fluid can vary a lot within different models, a common feature for several models is that the fluid can be described by a dynamical scalar field, bearing similarity to the inflation field. A general scalar field model of this type is referred here as the *quintessence* [13].

Now the action and the Lagrangian density for a generic scalar quintessence field Q are defined as:

$$S = \int \mathrm{d}^4x\sqrt{-g}\mathcal{L}_Q\,, \qquad \mathcal{L}_Q = -\frac{1}{2}g_{\mu\nu}\partial^\mu Q\partial^\nu Q + V(Q), \tag{2.13}$$

where g is the determinant of the metric tensor and $V(Q)$ is some unspecified potential, which in the end defines the evolution of the Q-field. The equations of motion of the Q-field again follow from the Euler-Lagrange equations:

$$\ddot{Q} + 3H\dot{Q} + V'(Q) = 0, \tag{2.14}$$

where the field was assumed to be homogeneous. The dot denotes the time derivative and $V' \equiv \frac{\mathrm{d}V}{\mathrm{d}Q}$. Using $\sqrt{-g}T_{\mu\nu} = -2\delta S/\delta g^{\mu\nu}$ the energy momentum tensor components for quintessence can be calculated. Comparing these with the energy momentum tensor of the ideal fluid $T^0_0 = \rho_Q$ and $T^i_i = -p_Q$, one finds the equation of state of the quintessence:

$$\omega_Q = \frac{p_Q}{\rho_Q} = \frac{\frac{1}{2}\dot{Q}^2 - V(Q)}{\frac{1}{2}\dot{Q}^2 + V(Q)}. \tag{2.15}$$

Since the $\omega_Q(t)$ parameter is time dependent, the apparent cosmological constant is actually a dynamical parameter in quintessence models.

As mentioned above, the form of the potential $V(Q)$ defines the evolution of the quintessence field and thus that of the dark energy. In this thesis the main interest is not in the specific quintessence models however, and the exact form of the potential is actually irrelevant here. Still the evolution of the Q-field needs to fit to the observations. It is also natural to assume that the field is not fixed to the potential minimum at the beginning, because in this case the quintessence would reduce to the ordinary cosmological constant. It can then be assumed that at some point $\dot{Q} \neq 0$, and because $V(t_0)$ is very small at the moment,

it is plausible that kinetic term of the Q-field dominates the energy density of the quintessence at some stage. Indeed, when $V'(Q) \ll 3H\dot{Q}$, it follows from Eq. (2.14) that $\dot{Q} \propto a^{-3}$, and moreover that the energy density scales as

$$\rho_Q \simeq \frac{1}{2}\dot{Q}^2 \propto a^{-6}. \tag{2.16}$$

This scaling is called *kination* [14]. It is relevant to notice that although kination can dominate the early universe expansion it must be over by the time of BBN, since otherwise it would dramatically alter the nucleosynthesis predictions of light element abundances in contradiction with observations. Yet the boosted expansion, if occurring much earlier than BBN, can be perfectly accepted, and might affect to the densities of heavy thermal relics, in some cases making them possible dark matter candidates. This scenario will be considered further later in this chapter.

2.2 Astrophysical evidence for the dark matter

The first astrophysical observations of support the existence of dark matter were made already in early 1930's.

In 1932 J. H. Oort [15] measured the velocities of stars in our galactic neighborhood and to explain why the stars were not flying away from the galactic plane he proposed that there must exist some dark matter to bound them into the system. This was the first indication of the dark matter but of course at that time there was yet no evidence for non-baryonic dark matter.

In 1933 F. Zwicky [16,18] measured radial velocities of galaxies belonging to Coma galaxy cluster and from these he was able to make a crude estimate of the total mass of the cluster using the virial theorem. Then he estimated the mass-to-light ratios of some nearby spiral galaxies and compared them to the mass-to-light ratios of the clusters and found that the ratio for the cluster was about 400 times larger than for the spirals (This result has since been verified, although the mass estimate has been improved). From this Zwicky concluded that the cluster needs to contain some non-luminous matter so that the observed motions of the galaxies could be understood.

Much later, in 1974, Ostriker et al. and Einesto et al. proposed that spiral galaxies are embedded in the dark matter halos, whose radii are several times larger than the size of the visible part of the galaxies. This picture was and still is in a good agreement with the observations; today there are several observations of the galaxy motions in galaxy groups, galaxy clusters and in superclusters which all point to the existence of dark matter. (For a recent review see [19].)

2.2.1 Galactic rotation curves

One of the first, and maybe the most convincing evidence for the dark matter follows from the measurements of the stellar rotation velocities in the spiral

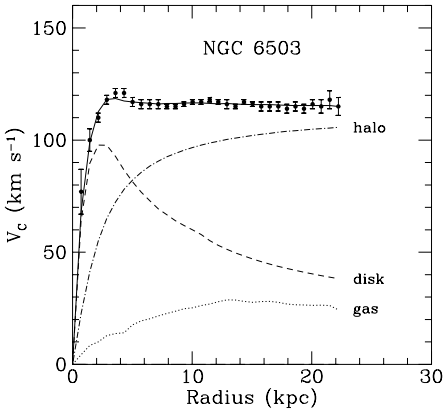

Figure 2.1: Example of spiral galaxy rotation curve. Galactic rotation curve for NGC 6503 showing disk and gas contribution plus the dark matter halo contribution needed to match the data. Picture adopted from [17].

galaxies. From the observed rotation velocities it easy to estimate the mass of the galaxy inside the radius of the orbit of the star using the Newton gravity. Indeed, according to Newtons theory a test particle on a circular orbit of a radius r from the center of a spherically symmetric matter distribution has a rotation velocity v;

$$\frac{v^2}{r} = \frac{G_N M(r)}{r^2} \qquad \Rightarrow \qquad v = \sqrt{\frac{G_N M(r)}{r}}\,, \tag{2.17}$$

where $M(r)$ is the mass inside the radius r and G_N is the Newton constant. So if the rotation velocities are measured then the mass can be calculated. On the other hand the mass of the visible galaxy can be estimated by counting and estimating the mass of the individual stars, gas and dust clouds. Thus the rotation velocity curve following from the mass distribution of the visible galaxy can be derived. The Keplerian velocity scaling law $v \sim 1/\sqrt{r}$ corresponding to a pointlike mass distribution, is easily seen from equation (2.17) when $M(r) = M = \text{const}$. This scaling law fits very well the measured rotation velocities of the planets in the solar system. One would expect that this law would hold at least fairly well also for star orbiting on near the edges of the visible galaxy. Yet the scaling law is not observed in galactic scales. Instead, the rotation velocities turn to a constant at the outskirts of the visible galaxy and continue to stay constant far beyond the visible disk. An example of galactic rotation curve showing this feature is shown in Fig. 2.1. Thus galaxies seem to be missing relatively large amounts of mass, supporting the existence of dark matter.

Conversely, from the observations of rotation curves one can solve the density distribution of the dark matter. Because the velocity profile turns constant at

large distances, the Newton theory prediction for the mass profile becomes

$$v^2 = \frac{G_N M(r)}{r} = \text{const.} \qquad \Rightarrow \qquad M(r) \propto r\,. \tag{2.18}$$

From this the density profile can be easily solved

$$\text{const.} = \frac{\mathrm{d}M(r)}{\mathrm{d}r} = 4\pi r^2 \rho(r) \qquad \Rightarrow \qquad \rho(r) \propto \frac{1}{r^2}\,. \tag{2.19}$$

Thus the dark matter halo enclosing the visible galaxy is expected to have this density profile called Singular Isothermal Sphere (SIS) (ref. [18] 4.4.3b). Remarkably this distribution is just what one would expect to find if the halo were formed of thermally distributed non-interacting dust-like particles.

Indeed, assuming that DM is a gas made of neutral, non-relativistic and collisionless particles, and further realizing that the dark matter halo formation is a very slow process, a simple model for dark matter halo formation can be built using the isothermal ideal gas law for the dark matter:

$$pV = Nk_BT \qquad \Rightarrow \qquad p(r) = \frac{\rho(r)}{m} k_B T\,. \tag{2.20}$$

Studying a differential gas volume element, the pressure-gravity equilibrium gives

$$\frac{\mathrm{d}p}{\mathrm{d}r} = -\frac{G_N M(r)\rho(r)}{r^2} \qquad \Rightarrow \qquad \frac{k_B T}{G_N m}\frac{\mathrm{d}}{\mathrm{d}r}\left(\frac{r^2}{\rho}\frac{\mathrm{d}\rho}{\mathrm{d}r}\right) = -4\pi\rho r^2\,, \tag{2.21}$$

where in the last step the Eq. (2.20) was used and the differentiation with respect to r was made, using the Eq. (2.19) for the mass differential. Eq. (2.21) is easily solved by a power function $\rho = Ar^b$, where A and b are constants, that are solved by direct substitution. One finds

$$\rho = \frac{\sigma^2}{2\pi G_N} r^{-2}\,, \qquad \sigma^2 \equiv \frac{k_B T}{m}\,. \tag{2.22}$$

Where the 1D velocity dispersion defined as $\sigma^2 \equiv \langle v_i^2 \rangle = \frac{1}{3}v^2 = k_b T/m$ was used to parametrize the solution. Although the halo formation in reality is a more complicated process, this simple model is fairly well consistent with the observations and thus can assumed to be good a approximation for the dark matter halo formation independent of the exact nature of the dark matter particles.

In summary, the observed flattening of rotation curves of spiral galaxies and their explanation with the help of halo made of noninteracting dark matter is one of the most convincing evidence for the existence of dark matter.

2.2.2 Structure formation

The present observable universe abounds in structure. The density contrast between the average empty space around us and the solar density is $\delta_\odot \equiv (\rho_\odot - \bar{\rho})/\bar{\rho} \sim 10^{30}$. Similarly in a typical galaxy, like Milky Way, the density contrast is of the order $\delta_{\rm gal} \sim 10^5$ and further in a galaxy clusters $\delta_{\rm clu} \sim 10^2 - 10^3$. Although the density contrast gets smaller the larger scale is viewed[4], there still is structure in all scales. How was all the structure formed? The answer lies in the cosmic microwave background radiation, that represents the state of the 380000 year old universe. The small temperature fluctuations of order $\delta T/T \sim 10^{-5}$, seen in the CMB spectrum were created by the density fluctuations in the plasma during the recombination and these fluctuations were the seed for the structures we observe today. The way the structures evolve from the ripples seen in the CMB spectrum to the observed large density constraints, is a highly complicated matter, which is beyond the scope of this introduction. However, it is known that if all the matter in the universe was made of baryons the observed structures could not have been formed in the time given. Instead, another pressureless matter component, decoupled from radiation is needed, which starts to build structures immediately after the matter-radiation equality via gravitational interactions. When the baryon-gas eventually decouples from photons, baryons fall into the potential wells already formed by this other matter component, increasing the efficiency of the structure formation. It thus appears that observed structures can only be explained by the interplay of some non-baryonic and baryonic matter components. This picture is consistent with the ΛCDM-model which includes the pressureless non-baryonic cold dark matter (CDM) component.

To summarize, motions of the galaxies in galaxy groups, galaxy clusters and larger structures as well as the rotation curves of the spiral galaxies indicate the presence of a sizable dark matter component. Furthermore, the structure formation and the WMAP results heavily support the existence of non-baryonic preasureless DM. Thus, there is a lot of observational evidence for the dark matter and in the next section the nature of this DM will be discussed.

2.2.3 Nature of the dark matter

The exact nature of DM is still unknown, although several candidates have been studied, among which new elementary particles are perhaps the most favorable ones. In general particle dark matter is categorized in to two classes; the *thermal* and *non-thermal* relics. The thermal DM particles are decoupled from the thermal path formed by the hot plasma in the early universe. The non-thermal DM particles, in general, have so weak interactions that they are never in equi-

[4]For example the quasar survey [2] shows that in large scales universe is rather homogeneous and isotropic.

librium. They can be created in some non-thermal process in the early universe, perhaps related to the end of the inflation or to some phase transition.

Further, the thermal particles are called either *hot dark matter* (HDM) or *cold dark matter*(CDM) depending whether they were relativistic or non-relativistic, respectively, at the moment of decoupling. For example the light SM neutrinos are hot dark matter, while the massive supersymmetric neutralinos would be cold dark matter and the axion field (particle) can be considered a non-thermal relic.

If the dark matter is hot it has specific influences on structure formation which are observationally constrained, because the energy density of a relativistic HDM can diffuse to large scales and wash away the small scale density contrast. This *free streaming* limits the amount of the hot dark matter that can exist, based on the the observed magnitude of the small scale structures in the galaxy distribution. Cold dark matter on the other hand clusters more efficiently thus remarkably helping to explain the structures seen in present universe, as was already mentioned above in connection with the structure formation.

DM particles in general can be either bosons or fermions. Fermions on the other hand can be either Dirac- or Majorana states depending on the structure of their mass matrix. They can have pure Dirac or Majorana mass terms or both, which through mass mixing results in Majorana states. Performing collision matrix element calculations with Majorana particles is more tricky than with Dirac particles, especially when mixing Majorana fields are considered. This is so because Majorana particles are their own antiparticles, which increases the number of non-trivial contractions. Moreover for mixing fields comprehensive Feynman rules are still lacking. There are new aspects associated with the phases of the mixing Majorana fields, whose effects to the cross section and relic density calculations, and to particle physics considering mixing fields in general has not yet been fully appreciated in the literature. Clearing these issues is one of the main results in this thesis. These issues will be considered in more detail in Sec. 4.4 and in Appendix where an example calculation of matrix element including mixing Majorana fields is given.

Before going further with the hot/cold particle dark matter scenarios let us consider baryons and their role as dark matter.

Baryons as dark matter

If we ignored the WMAP results for the matter content of the universe and considered only the galaxy cluster motions and galaxies rotation curves as a evidence of dark matter, the first natural assumption would be that the dark matter is made of non-luminous baryons. Indeed, all the visible matter is made of baryons, although the stars and hot gas yields only small fraction of the total energy density of the universe: $\Omega_b^{lum} \approx 0.003$ [20]. The rest of the baryonic matter predicted by the BBN ($\Omega_b^{tot} \approx 0.04$) should then be in a non-luminous form i.e. dark, and observable only through the gravitational effects. This dark

baryonic matter could be for example in the form of a gas, dust, (primordial) black holes or other faint massive compact objects.

However, the amount of baryons predicted by the BBN is not enough to make the universe flat and this contradicts the inflation prediction. This sets the first doubts over the pure baryonic dark matter.

Hiding large amounts of baryons to ionized or neutral *gas* is also very difficult. This is easily verified using the SIS model. Indeed, assuming that all the missing mass in a galaxy is in the form of a baryonic gas (mostly Hydrogen $m \approx m_p$), the temperature of the gas can be computed using Eq. (2.19) and Eq. (2.22), which give

$$\text{const.} = \frac{M(r)}{r} = \frac{2k_B T}{m_p G_N}\,. \tag{2.23}$$

Substituting typical galactic (Milky Way) scales to the equation one finds the temperature

$$T \approx 230\,\text{eV}\left(\frac{\text{M}}{10^{12}\text{M}_\odot}\right)\left(\frac{100\text{kpc}}{\text{R}_{\text{halo}}}\right)\,. \tag{2.24}$$

Baryonic gas of this temperature should radiate photons in the X-ray region so brightly that it would have been already detected with present telescopes.

Further, according to observations the *dust* is expected to form only $\Omega_{dust} \lesssim 2\times10^{-6}$ of the total energy density [21]. The *massive compact halo objects* (MACHOs), such as black holes and faint objects such as Jupiters, brown dwarfs or white dwarfs ranging from planetary to stellar masses have been search by MACHO [22] and EROS [23] collaborations. Their results indicate that MACHOs can cover at most 20% of the Milky Way halo mass and that MACHOs in mass range $10^{-7}M_\odot - 20M_\odot$ are excluded as a primary constituents in Milky Way halo. It is reasonable to think that this trend follows also to larger scales, which suggests that the MACHOs are not the dominant the dark matter component in the universe.

The *black holes* can be formed either at deaths of massive stars or in the early universe, for example in the QCD-phase transition. The black holes which are star remnants should obviously be formed out of baryonic dark matter whereas the primordial black holes could be also considered as CDM. If all the dark matter were made of black holes formed in supernovaes, one would expect that the heavy elements would be much more abundant than what has been observed, since in this case large amount of light elements would have gone trough the stellar cycle ending up in formation of heavier elements. The primordial black holes have also other constraints [25]. In particular they must have been massive enough when formed so that they would not have evaporated by now. There are mass regions where black holes could be the dark matter but then, according to [26], the primordial black holes need to be either the dominant dark matter component or, if also a particle dark matter component exists, the black hole dark matter is constrained to form only small fraction of the total density $\Omega_{PBH} \lesssim \times10^{-4}$. (Otherwise the annihilating WIMPs, which are assumed to ac-

crete a ultracompact minihalos around the PBH's, would produce an observable annihilation end-product signal [26].)

These observations, which are supported by WMAP results, show that baryons cannot explain the total mass observed in the universe. In addition it is concluded that part of the baryonic matter seems to be missing.

Hot dark matter

Another group of candidates for the dark matter are the SM light neutrinos. These neutrinos were relativistic at the time of the decoupling so they are considered as hot relics. Yet, if their mass exceeds the $\sim 10^{-4}$ eV, which is the current cosmic neutrino background temperature, these neutrinos are non-relativistic today. In cosmology the sum of the masses of the neutrinos becomes the most relavant parameter, in particular because the structure formation is affected by the neutrino energy density because of the free streaming. This highly constrains the total amount of light neutrino dark matter, setting $\sum_\nu m_\nu \lesssim 0.6 - 0.7$eV, which implies that (using the dimensionless Hubble parameter $h = 0.71$) the current dark matter density coming from light neutrinos is limited by the precision cosmology data to $\Omega_\nu \lesssim 0.015$ [27].

Another well motivated dark matter candidate, which like baryons is related to Quantum Chromodynamics (motivated by the model introduced to fix the strong CP-problem) is the pseudoscalar axion field (see e.g. [28]). There are mechanisms to produce this pseudoscalar axion thermally or non-thermally. Recent analysis considering several distinct cosmic data sets [29] show that thermally produced axions should be considered as a hot dark matter ($m_a \lesssim 0.91$ eV at 95% C.L.) but in this case they cannot explain all the missing mass in the universe because of the free streaming constraint which affects them in the same way as it affects light neutrinos. However if axions were produced non-thermally, (even though in this case the axions are even lighter, $m_a \lesssim \mu$eV) they can be threated like cold dark matter since the momentum of the axion condensate is essentially zero. Such light axion is still a viable dark matter candidate.

Other possibilities: MOND?

After going through the obvious dark matter candidates included in the standard model of particle physics one might change the line of thinking and ask if the solution to the DM problem could be that there is something wrong with the Newton gravity. Maybe the Newton gravity does not work correctly at large distances so that to explain the observation one should modify the Newton gravity theory. These kind of theories have been developed and they are called Modified Newtonian Dynamics MOND [30] (see short review e.g. [31]).

The MOND models are able to explain the galactic rotation curves using only the estimated mass of the visible baryonic matter in many cases. Yet building a MOND which fits to all observations with fixed model parameters seems to

be problematic and especially explaining the motions of the galaxies in galaxy clusters and in larger systems seems to be difficult in the MOND models.

Also the N-body simulations of structure formation within MOND have been done. A generic problem within the MOND, according to Ref. [32], seems to be the late time of the structure formation meaning that although the present structures, similar to ΛCDM-model, can be formed using the MOND, the lack of structures in redshifts $z \geq 3$ contradicts the observation of structures at $z \sim 6$.

The first MOND models were also criticized by the fact that they did not respect the relativity principles, but relativistic MOND models have since been built. These models are generally very complicated and highly phenomenological, lacking sound independent theoretical motivation.

Gravitational lensing and the Bullet cluster

As is well known the general relativity, (as well as Newtonian gravity, although erroneusly) predicts the bending of the trajectory of the light as it travels by a massive object. This light bending phenomena is called *gravitational lensing* and it has been used in cosmology to study the shape of matter distribution in the universe. Especially it has been used to reveal the existence, the amount and the nature of the dark matter [34].

In gravitational lensing the image and the brightness of a light emitting source; a star, a galaxy etc., depend on the mass, the shape and the size of the object or objects which work as a lens, and also on the distances from the source to the observer and to the lens. Thus information of the lensing object is gained from analyzing the images of known light sources. Depending on the shape and the size of the lensing objects different names for the lensing phenomenon are used. The term *strong lensing* is used when the lens is massive and a fairly compact object like a core of a galaxy or a galaxy cluster, and multiple images of the source are seen. *Microlensing* refers mainly to the MACHO searches in galactic halo. In this case the identification of the lens is based on the brightening of the source, usually a star, and not on detection of separate images. Most of the light propagating trough the universe, along the line of sight, does not pass near any strong lenses however. Even this light can be deflected slightly when it passes far from the core of a galaxy or a galaxy cluster in general or through a weak gravitational field. This *weak lensing* phenomenon is used to study the average dark matter distribution in large scales and the dark matter density in the universe. Weak lensing results are in a nice agreement with the WMAP results supporting the ΛCDM-model and when combined yielding $\Omega_m = 0.248 \pm 0.019$ [35].

The weak lensing plays important role also in the so called *bullet cluster* observation [36], which arguably verifies the existence of the dark matter and rules out the MOND models. The bullet cluster refers to an unvirialized system of two colliding clusters of galaxies, imaged by three different observational meth-

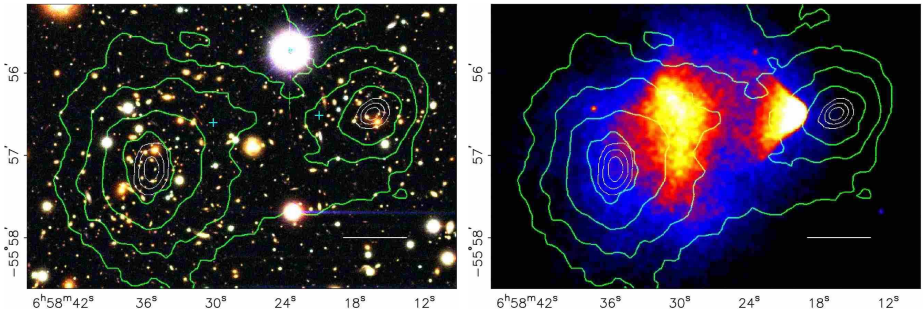

Figure 2.2: The bullet cluster. In left picture the visible collided clusters with the (green) gravitational equipotential contours adopted by the weak lensing. In right picture the same figure but now the X-ray instead of visible band is shown. Pictures taken from [36].

ods to determine the different mass components in the system Fig. 2.2. The optical image reveals the visible mass in the system, the X-ray image shows the distribution of the hot ionized gas which was collected together and heated in the collision. Finally, the weak lensing image shows the constant gravitational potential contours created by the total mass concentrations in the clusters. The mass belonging to the gas is dominating over the mass of stars in the galaxies in the clusters, and so it would be expected that the center of the gravity well should coincide with in the center of the accumulated hot gas. However the weak lensing results clearly indicate that the centers of the mass distributions are following the visible galaxy clusters. This observation is consistent with the existence of weakly interacting dark matter which, just like the stars in the galaxies pass through without interacting in the cluster collision, so that the dark matter distribution follows the distribution of the visible galaxies. However, MOND models where the observations are considered to be explained by baryons only, the center of the gravity potentials should follow the dominant gas component, which is in contradiction with the two mass centers observed by lensing observations. Thus the bullet cluster observation seems to verify of existence of collisionless dark matter and rule out the MOND.

Cold dark matter

The indirect and the lack of direct observations indicate that dark matter should be made of massive weakly interacting particles WIMPs. Since WIMPs are non-relativistic and weakly interacting, a halo made of WIMPs can be modeled with the isothermal ideal gas law naturally giving rise to the desired SIS density profile. The fact that the SIS model is consistent with both the N-body dark matter simulations for the dark matter halo profiles and with the actual observations improves the status of CDM and the WIMP scenarios as a correct solution for the dark matter problem.

The favorite dark matter particle or WIMP is the lightest supersymmetric particle (LSP). Typically LSP is expected to be a neutralino which is mixture of the neutral SUSY states, mostly bino or photino. The stability of the LSP is guaranteed by a postulated new symmetry; the R-parity and the associated conserved quantum number, which is +1 for SM particles and -1 for their SUSY partners. Other WIMP candidates proposed over the years include massive non-SM neutrinos such as the fourth family heavy neutrinos, a variant of which is studied in this thesis and detailed in articles [I] and [II]. These states are naturally predicted by the minimal walking technicolor theory which is discussed in more detail in next the chapter. The DM aspects of heavy neutrinos have been earlier considered also in [38, 39]. The recent advanced technicolor models provide also other cold dark matter candidates such as the TIMP introduced in [40–42] and other exotics [43] which are techni-interacting. Many other cold dark matter particle candidates with different origins and production mechanisms, having wide range of masses and interaction strengths and specific signatures have been proposed. Yet, few of them have equally sound theoretical basis as the LSP and the technicolor based WIMPs considered in this thesis.

Although WIMPs have not been directly detected yet, the experiments have started to put interesting constrains on the parameter space of the WIMP models. The improved experimental efficiencies set also demands to the DM models. The DM models need to be complete or otherwise well defined so that their predictions can be calculated to high precision. These include the WIMP-nucleon cross sections, which are constrained by the direct cryogenic DM search experiments, the possible WIMP accumulation and annihilation in the core of the Earth, the Sun or the Galaxy, which can be searched by observation of the WIMP-annihilation end-products in the indirect DM searches. Lastly, also the direct collider signals should be determined. Of course the cosmic WIMP density needs to be solved first to test whether a correct amount of DM can be created in a given model. In the following section the equation from which the WIMP relic density can be solved is derived. The constrains to WIMP properties, which follow from observational DM searches, are considered in more detail in Sec. 4.6.

2.3 The Boltzmann equation

In the following the Boltzmann equation which describes the evolution of the number density of the thermal WIMPs will be derived [45–47]. Let us first study the effects of the expansion on the particle momentum. In microscopic scale the curvature is irrelevant and the early universe is taken to be effectively flat and described by the metric

$$\mathrm{d}s^2 = \mathrm{d}t^2 - a(t)^2(\mathrm{d}x^2 + \mathrm{d}y^2 + \mathrm{d}z^2), \tag{2.25}$$

where $a(t)$ is the scale factor as before and t, x, y, z are the co-moving coordinates. By minimizing the action for the path length:

$$S = \frac{1}{2}\int \mathrm{d}\lambda \mathcal{L}\,, \qquad \mathcal{L} \equiv \frac{\mathrm{d}s^2}{\mathrm{d}\lambda^2}, \tag{2.26}$$

where λ is arbitrary affine parameter, the Euler-Lagrange equations, particle trajectory (geodesic), can be calculated:

$$\frac{\mathrm{d}^2 t}{\mathrm{d}\lambda^2} = -a\dot{a}\Big(\frac{\mathrm{d}\vec{x}}{\mathrm{d}\lambda}\Big)^2, \qquad \frac{\mathrm{d}^2 x^i}{\mathrm{d}\lambda^2} = -2\Big(\frac{\dot{a}}{a}\Big)\frac{\mathrm{d}t}{\mathrm{d}\lambda}\frac{\mathrm{d}x^i}{\mathrm{d}\lambda}, \tag{2.27}$$

where $\vec{x} = (x, y, z)$ and dot denotes the time derivative. Now define the four-momentum in the co-moving coordinates as $p_c^\mu \equiv \mathrm{d}x^\mu/\mathrm{d}\lambda$. This differs from the four-momentum p^μ measured at the local orthonormal coordinates corresponding to the flat metric $\eta_{\mu\nu} = \mathrm{diag}(1, -1, -1, -1)$ in which the usual quantum field theory rules are formulated. Since the p^2 does not depend on the coordinate system $p^2 = p_c^2$, from which it follows that: $E = E_c \equiv \mathrm{d}t/\mathrm{d}\lambda$ and $\vec{p} = a\vec{p_c}$. Thus, using the previous definitions and relations with Eq. (2.27) the λ-derivatives of the momentum and the energy can be solved in local orthonormal coordinates;

$$\begin{aligned} \frac{\mathrm{d}\vec{p_c}}{\mathrm{d}\lambda} = -2\frac{\dot{a}}{a}E_c\vec{p_c} \quad &\Longrightarrow \quad \frac{\mathrm{d}\vec{p}}{\mathrm{d}\lambda} = -\frac{\dot{a}}{a}E\vec{p}, \\ \underbrace{\frac{\mathrm{d}E_c}{\mathrm{d}\lambda} = -a\dot{a}\vec{p_c}^{\,2}}_{\textit{co-moving}} \quad &\Longrightarrow \quad \underbrace{\frac{\mathrm{d}E}{\mathrm{d}\lambda} = -\frac{\dot{a}}{a}\vec{p}^{\,2}}_{\textit{local orthonormal}}. \end{aligned} \tag{2.28}$$

These evolution equations can be used for interacting particles in an expanding universe and are needed in the following derivation of the Boltzmann equation.

The Boltzmann equation describes the evolution of the phase-space density of the WIMPs, which in general is of the form $\hat{f}(x^\mu(\lambda), p^\mu(\lambda))$ [5]. In an FLRW universe the density distribution is spatially homogeneous and isotropic however, so that $\nabla_{\vec{x}}\hat{f} = 0$. In the non-interacting case the density is of course constant along geodesics so that $\mathrm{d}\hat{f}/\mathrm{d}\lambda = 0$, which using the Einstein chain rule and equations (2.28) becomes:

$$\begin{aligned} \frac{\mathrm{d}\hat{f}}{\mathrm{d}\lambda} &= \frac{\mathrm{d}t}{\mathrm{d}\lambda}\frac{\partial}{\partial t}\hat{f} + \frac{\mathrm{d}\vec{p}}{\mathrm{d}\lambda}\cdot\nabla_{\vec{p}}\hat{f} + \frac{\mathrm{d}p_0}{\mathrm{d}\lambda}\frac{\partial}{\partial p_0}\hat{f} \\ &= p_0\frac{\partial}{\partial t}\hat{f} - \frac{\dot{a}}{a}p_0\vec{p}\cdot\nabla_{\vec{p}}\hat{f} - \frac{\dot{a}}{a}\vec{p}^{\,2}\frac{\partial}{\partial p_0}\hat{f} \\ &= 0\,. \end{aligned} \tag{2.29}$$

Otherwise the fluctuations in the density follow from the interactions with other particles; $\mathrm{d}\hat{f}/\mathrm{d}\lambda = \hat{C}(p, t)$, where the collision term $\hat{C}(p, t)$ describes the interactions with the background. The physical phase-space density is defined on

[5] The system is described in local orthonormal coordinates and the effects of expansion are fed in through the evolution equations (2.28). Other approach, starting with co-moving coordinates, has been followed e.g. in Ref. [45].

(positive) mass-shell however. That is by

$$f(p,t) = \int_0^\infty \hat{f}(p_0, \vec{p}, t)\delta(p_0 - (\vec{p}^2 + m^2)^{1/2})\mathrm{d}p_0\,, \tag{2.30}$$

where the dependence of only $p \equiv |\vec{p}|$ and t follows from isotropy and homogeneity requirements. Thus the mass-shell integral to be studied is of the form:

$$\int_0^\infty \frac{\mathrm{d}\hat{f}}{\mathrm{d}\lambda} 2\delta(p^2 - m^2)\mathrm{d}p_0 = \int_0^\infty \frac{\mathrm{d}\hat{f}}{\mathrm{d}\lambda}\frac{1}{p_0}\delta(p_0 - (\vec{p}^2 + m^2)^{1/2})\mathrm{d}p_0\,, \tag{2.31}$$

from which the Boltzmann equation directly follows by using $\mathrm{d}\hat{f}/\mathrm{d}\lambda = \hat{C}(p,t)$ with Eq. (2.29) and Eq. (2.30):

$$\frac{\partial}{\partial t}f - \frac{\dot{a}}{a}\vec{p}\cdot\nabla_{\vec{p}}f = \int_0^\infty \hat{C}(p,t)\frac{1}{p_0}\delta(p_0 - (\vec{p}^2 + m^2)^{1/2})\mathrm{d}p_0\,. \tag{2.32}$$

Integrating Eq. (2.32) over the momentum p and using partial integration the usual form of the integrated Boltzmann equation is found:

$$\dot{n}(t) + 3H(t)n(t) = g\int \frac{\mathrm{d}^3p}{(2\pi)^3}\frac{1}{E}C(p,t). \tag{2.33}$$

Here $n(t) = g\int \frac{d^3p}{(2\pi)^3}f(p,t)$ is the particle number density, where g counts the particle species internal degrees of freedom and $H(t) = \dot{a}/a$ the Hubble parameter. The $C(p,t)$ is interaction term containing the elastic and inelastic collision integrals. From Eq. (2.33) it can be seen that in the absence of collisions ($C(p,t) = 0$) the particle number density merely gets diluted because of the expansion of the universe, so that the solution for the Boltzmann equation in this case is $n \sim a^{-3}$.

2.3.1 Lee-Weinberg approximation

Beyond having integrated the original Boltzmann equation over the 3-momenta, other simplifications are possible when studying thermally decoupling dark matter. First assume that particles are held in kinetic equilibrium by elastic scatterings. Further assume that the 2→2 particle processes dominate the inelastic interactions. Then the WIMP density evolution is mainly affected by the annihilations of the WIMPs to other particles. With these approximations[6] the collision integral in Eq. (2.33) can be written in form:

$$\begin{aligned} g\int \frac{\mathrm{d}^3p}{(2\pi)^3}\frac{1}{E}C(p,t) \;=\; & -\sum_i \int \mathrm{d}\Pi_\chi\,\mathrm{d}\Pi_{\bar{\chi}}\,\mathrm{d}\Pi_i\,\mathrm{d}\Pi_{\bar{i}}\,(2\pi)^4\delta^4(p_\chi + p_{\bar{\chi}} - p_i - p_{\bar{i}}) \\ & \times\big[\,|\mathcal{M}|^2_{\chi+\bar{\chi}\to i+\bar{i}}\,f_\chi f_{\bar{\chi}}(1\pm f_i)(1\pm f_{\bar{i}}) \\ & \quad -|\mathcal{M}|^2_{i+\bar{i}\to\chi+\bar{\chi}}\,f_i f_{\bar{i}}(1\pm f_\chi)(1\pm f_{\bar{\chi}})\,\big], \end{aligned} \tag{2.34}$$

[6] See more about the Boltzmann equation and the approximations e.g. [46, 47, 53].

where the sum over i refers to all possible final state to which the WIMPs, denoted by χ, can annihilate. f_j is the phase space density of the species j and in the blocking factors + is for bosons and − for fermions. $|\mathcal{M}|^2_{a+b\to c+d}$ are the squared annihilation matrix elements for the processes $a+b\to c+d$ including the appropriate symmetry factors for the initial and final states and averaged over the initial and final state spins. Furthermore, the delta function ensures the momentum conservation and the invariant phase space volume elements are defined as $d\Pi_j \equiv \frac{g_j}{(2\pi)^3}\frac{d^3p_j}{2E_j}$. Now assuming time reversal invariance the same matrix element can be used for the inverse annihilation processes:

$$|\mathcal{M}|^2_{\chi+\bar{\chi}\to i+\bar{i}} = |\mathcal{M}|^2_{i+\bar{i}\to\chi+\bar{\chi}} \equiv |\mathcal{M}|^2. \tag{2.35}$$

Moreover, since the WIMPs are massive and non-relativistic at the time of decoupling, Maxwell-Boltzmann statistics can be used and the Fermi/Bose blocking/enhancement factors can be ignored: $1 \pm f_j \simeq 1$. (Also chemical potentials are assumed to be zero here.) Yet further, assuming that the kinetic equilibrium is always retained during the *freeze-out* process, the energy conservation $E_\chi + E_{\bar{\chi}} = E_i + E_{\bar{i}}$ sets a useful relation for the densities:

$$f_i f_{\bar{i}} = \exp[-(E_i + E_{\bar{i}})/T] = \exp[-(E_\chi + E_{\bar{\chi}})/T] = f^{eq}_\chi f^{eq}_{\bar{\chi}}, \tag{2.36}$$

where f^{eq}_χ is the thermal Maxwell equilibrium density distribution. With these approximations the collision integral reduces to [53]:

$$\begin{aligned} g\int \frac{d^3p}{(2\pi)^3}\frac{1}{E}C(p,t) &= -\sum_i \int d\Pi_\chi\, d\Pi_{\bar{\chi}}\, d\Pi_i\, d\Pi_{\bar{i}}\,(2\pi)^4\delta^4(p_\chi + p_{\bar{\chi}} - p_i - p_{\bar{i}}) \\ &\qquad \times|\mathcal{M}|^2[\, f_\chi f_{\bar{\chi}} - f^{eq}_\chi f^{eq}_{\bar{\chi}}\,] \\ &= -\langle v\sigma\rangle(n^2 - n^2_{eq})\,, \end{aligned} \tag{2.37}$$

where in the last line n_{eq} is the number density in thermal equilibrium and $\langle v\sigma\rangle$ is a velocity average total annihilation cross section which when the Maxwell-Boltzmann distribution is used to describe the DM particles becomes a simple 1-dimensional integral [53]:

$$\langle v\sigma\rangle = \frac{1}{8m^4TK_2^2(\frac{m}{T})}\int_{4m^2}^\infty \mathrm{d}s\sqrt{s}(s-4m^2)K_1(\frac{\sqrt{s}}{T})\sigma_{\rm tot}(s)\,. \tag{2.38}$$

Here $K_i(y)$'s are modified Bessel functions of the second kind and s is the usual Mandelstam invariant and T is temperature. The total annihilation cross section $\sigma_{\rm tot}(s)$ is the sum of the DM particle annihilation cross sections to all the possible final states. Thus the Boltzmann equation eventually reduces to familiar Lee-Weinberg equation [48]:

$$\dot{n} + 3Hn = -\langle v\sigma\rangle(n^2 - n^2_{eq}). \tag{2.39}$$

Changing the variables

$$x = b(T)\frac{T}{m}\,, \qquad f(x) = \frac{n(x)}{s}\,, \tag{2.40}$$

where

$$s = b(T)^3 T^3\,, \qquad b(T) = \Big(\frac{2\pi^2}{45} g_{*s}(T)\Big)^{1/3}\,,$$

and s is the entropy density, $g_{*s}(T)$ is the number of entropy degrees of freedom at the temperature T and m is the WIMP mass, Eq. (2.39) finally becomes

$$\frac{\partial f(x)}{\partial x} = \frac{\langle v\sigma\rangle m^3 x^2}{H(x)}(f^2(x) - f_{eq}^2(x))\,. \tag{2.41}$$

Given the Hubble parameter H (Eq. (2.43) below) and the average annihilation rate $\langle v\sigma\rangle$ (Eq. (2.38)) this equation can be solved numerically.

Hubble expansion parameter

For Hubble parameter in the early universe can be used the form

$$H^2 = \frac{8\pi G_N}{3}(\rho_{rad} + \rho_Q), \tag{2.42}$$

where the expansion is driven not only by the standard radiation density $\rho_{rad} = (\pi^2/30)g_*(T)T^4$, where $g_*(T)$ denotes the number of energy degrees of freedom at the temperature T, but also the dynamical dark energy part ρ_Q dominated by the kinetic energy term of generic quintessence field. The kination scaling law for the quintessence energy density is $\rho_Q \sim a^{-6}$. With the definitions from Eq. (2.40) and the entropy conservation in co-moving frame the above Hubble expansion formula can be written as

$$H = \bar{H}_0\Big(\frac{x}{x_0}\Big)^2 \Big(h + r\,\big(\frac{x}{x_0}\big)^2\Big)^{1/2}, \tag{2.43}$$

where $\bar{H}_0 = (8\pi\rho_{\mathrm{rad},0}/3M_{\mathrm{Pl}}^2)^{1/2}$ is the Hubble expansion rate at the reference temperature $T = T_0 \equiv 1$ MeV in the standard cosmology, $r \equiv \rho_{\phi,0}/\rho_{\mathrm{rad},0}$ is the ratio between dark energy and radiation energy densities at $T = T_0$ and $h \equiv (g_*(T)/g_*(T_0))(g_{s*}(T)/g_{s*}(T_0))^{4/3}$. Naturally if $r \equiv 0$ the standard radiation driven expansion is obtained. The standard expansion is usually considered when the annihilation cross section of the dark matter particles is suppressed with the mixing or is otherwise small. This is the case in articles [II] and [III]. However, in the article [I], where the WIMP has standard, unsuppressed weak interaction strength, the more general kination driven expansion law was used. The effects of the expansion and cross section to the WIMP density are explained

in more detail in subsection 2.3.2 below.

In article [I] Eq. (2.41) was solved analytically using approximative methods as in [39]. In articles [II] and [III] it was solved numerically using a specialized Fortran 95 code. Given the solution for Eq. (2.41) the density parameter for dark matter particles can be calculated from the value of the f-function today: $f(0)$ and the definitions in Eq. (2.40) and Eq. (2.10), resulting to

$$\Omega_{\rm DM} = a\frac{2mf(0)s_0}{\rho_{c,0}} \simeq 1.09 \times 10^9 a \left(\frac{m}{\rm GeV}\right) f(0)\,. \tag{2.44}$$

Here the subscript 0 refers to present values of quantities and $a = 1$ for Dirac particles and $a = 1/2$ for Majorana particles.

2.3.2 Annihilation rate vs. expansion rate

The largest effects on the final abundance of the thermal dark matter particles, described by Eq. (2.41), come from the Hubble parameter and from the annihilation cross section. The smaller the cross section, or the larger the expansion rate H, the larger final density is obtained. This is illustrated in Fig. 2.3, which describes generically the freeze-out process. Physically this can be understood so that the smaller the cross section is the longer it takes for particles to find an antiparticle with which to annihilate, and thus the particle density drops earlier from the equilibrium as the Hubble expansion overcomes the annihilation rate, and the universe becomes transparent for the DM particles (The mean free path of the WIMP becomes longer than the particle horizon.)

If one considers for example a standard model like $4^{\rm th}$ family heavy neutrino with standard weak interactions and a standard radiation driven expansion of the universe the outcome is that these neutrinos cannot work as a dark matter. The reason is that their cross sections is too large for allow a large enough relic density. But if the annihilation cross section was but an order or two magnitudes smaller or if the early universe expansion were enhanced by some mechanism these particles could be produced in suitable quantities to become a dominant dark matter component.

The usual method is to tweak the cross section by a mass mixing, so that the mixing angles suppress the WIMP couplings to SM fields. In addition to boosting the density this method has other favorable outcomes: for example as it makes the particles more weakly interacting, it helps to explain why these particles have escaped detection in the dark matter search experiments. Such WIMPs also produce weaker astrophysical signals. However, if the cross section were too small, the DM particles could be overproduced, so that they would make the universe closed in contradiction with observations. Thus achieving naturally just the right coupling strengths is a desired feature of any realistic dark matter model.

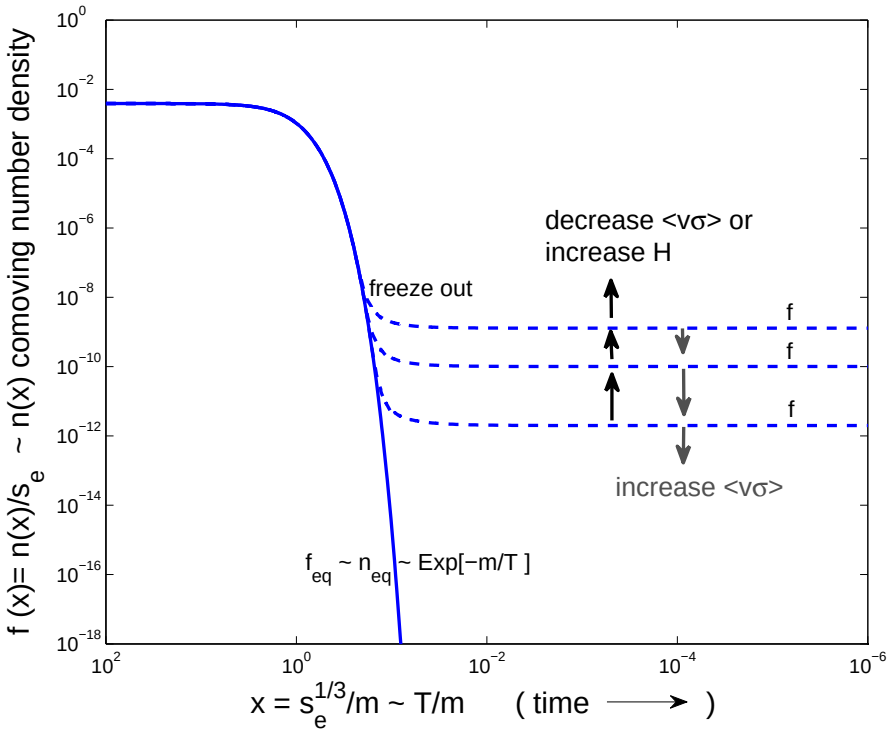

Figure 2.3: The freeze-out of a WIMP. Dashed line corresponds to the actual density of the WIMPs and solid line depicts the equilibrium density. The evolution of the WIMP density, when Hubble expansion is increased or annihilation cross section is suppressed, is illusterated.

Another possibility to produce a correct dark matter density is to effect a stronger expansion rate with some mechanism. In article [I] was considered a model where a dynamical dark energy, corresponding to a kinetic term of a quintessence scalar field, dominated the early universe expansion. (This idea for a generic WIMP was studied earlier in [49], and in the case of a scalar tensor gravity in [50].) The increased expansion makes DM particles decouple earlier from thermal bath increasing the relic density suitably. The early universe expansion cannot be modified arbitrarily, however. In particular the quintessence dominance must end before the big bang nucleosynthesis so that the light element abundances, which according to observations support the standard BBN theory, are not changed too much. Nevertheless, the expansion law can be adjusted to provide both the correct DM abundance and the successful BBN. However the model now appears to be ruled out. The problem is that since the couplings to SM fields are not suppressed, the particles have difficulties to escape from being detected by the direct dark matter search experiments. Only if the local dark matter density is estimated drastically wrong (which is fairly unlike [51]) or that these particles are extremely heavy, this scenario could be still possible. Otherwise the DM particles with standard weak interactions to SM fields are ruled out by the direct DM search experiments [52].

Chapter 3

Technicolor

In this chapter a brief motivation and introduction to Technicolor (TC) and to Extended Technicolor (ETC) is given. Then a Minimal Walking Technicolor (MWT) model and its minimal extension are presented and discussed as sources of dark matter.

3.1 Motivation

The Standard Model of elementary particle physics (SM) is a combination of the Quantum Chromodynamics (QCD) and the Electroweak (EW) Glashow-Weinberg-Salam theory, with the gauge structure $SU(3) \times SU(2) \times U(1)$. It successively predicts a vast number of different physical phenomena, and yet there are a few important observations and internal issues that remain unexplained. Three of these are related to studies presented in this thesis:

- The hierarchy and naturality problems i.e. why is the Higgs mass scale that of the EW scale ($\sim$ 100 GeV); why is the EW symmetry breaking happening at that scale, although in the renormalization picture the natural scale for the scalar field mass term is the ultraviolet cut off scale, which in the SM is naturally of the order of the Planck scale ($\sim 10^{18}$ GeV)?

- The dark matter problem i.e. what is that dark matter which seems to dominate the matter content of the universe?

- Why there are so many different forces in SM i.e. why there are three gauge groups with different coupling constants in the SM? Could these be unified as a grand unified theory (GUT) at very high energies, under a single large group with one coupling constant?

Finding the answers to the hierarchy and naturality problems is the main motivation for the technicolor. The possible answers to the latter two questions are discussed in the end of this chapter and partly in the next chapter.

The original Higgs mechanism of obtaining the electroweak symmetry breaking (EWSB) in the SM is very simple. What is needed are just some new fields that are coupled to weak gauge bosons and a mechanism which breaks the local $SU(2) \times U(1)$ symmetry to U(1) electromagnetism, however such that a global SU(2) symmetry is conserved; this *custodial symmetry* guarantees the right mass ratio for the massive EW gauge bosons.

In the standard Higgs scenario the weak gauge bosons are coupled to a complex scalar doublet whose potential is chosen so that it obtains a non-zero vacuum expectation value (VEV) which breaks the local SU(2) gauge symmetry. Before symmetry breaking the scalar degrees of freedom in the Higgs doublet, when considered as a four real scalar fields, have a global O(4) symmetry. In the symmetry breaking this breaks to O(3), which has precisely the algebra of the custodial SU(2) symmetry. The same phenomenon happens also in two flavor QCD, from which the idea was adopted to TC at higher energies.

Indeed, in the two flavor QCD the approximately massless quarks have a left-right chiral symmetry. The left handed u and d quarks forming an SU(2) doublet which is coupled to weak gauge bosons and the right handed states form another doublet with just a global SU(2) symmetry. At high energies, well above $\Lambda_{\mathrm{QCD}} \sim 200\mathrm{MeV}$, the system has eight symmetries with the corresponding symmetry currents. When the energy drops and becomes of the order of, or less than Λ_{QCD}, the QCD coupling becomes strong and the quarks form a condensate. This condensate breaks the local SU(2) symmetry and the goldstone bosons (the pions) from the broken axial-isospin symmetry are left to be eaten by the EW gauge bosons if it would be considered that there was no Higgs field and no Higgs mechanism. Yet the global SU(2) isospin current is not broken and this custodial symmetry guarantees the right mass ratio for the weak gauge bosons. The mass scale ($\sim \Lambda_{\mathrm{QCD}}$) of the gauge bosons is of course too small in this case.

Technicolor copies this mechanism by introducing a new strong gauge interaction TC and new chiral techniquarks on which the TC interactions acts, and by requiring that the TC coupling becomes strong at the EW energy scale $\Lambda_{\mathrm{TC}} \sim 100 - 1000$ GeV, the EWSB could be achieved dynamically without the problems associated with the fundamental scalar Higgs field.

The following introduction to the TC and the extended technicolor follows reviews by Hill and Simmons [54] and by Sannino [55].

3.2 Introduction to TC and ETC

Technicolor is an alternative for the SM Higgs sector for the electroweak symmetry breaking. As explained above, TC is a new QCD-like strongly interacting gauge theory involving new chiral fermions (techniquarks) that feel a new gauge interaction (technicolor). The EW energy scale is the fundamental energy scale in which the TC interactions become so strong that the technifermions will form a condensate breaking EW symmetry according to the desired pattern. The

excitations of this condensate can be interpreted as a composite Higgs. The formation of this condensate introduces a dynamical EWSB without the fine-tuning issues associated with the fundamental scalar Higgs fields.

Although this way of solving the hierarchy problem is very elegant TC contains also some issues which need to be solved before it can become a credible theory for EWSB. In summary these are: consistency with the EW precision data, acceptable Goldstone boson masses, suppression of flavor changing neutral currents and generation of the fermion masses.

When the SM Higgs is replaced with a techniquark condensate, a composite Higgs, the theory and it predictions change. Question then is, whether the new theory is consistent with the experimental data? For example new fermions related to the TC-model, when coupled to EW-boson, change the weak gauge boson vacuum polarization amplitudes, which are usually parameterized with the *oblique parameters* S,T and U. These on the other hand are highly constrained by the EW precision data from LEP II. Since the SM predictions for S,T and U are in good agreement with the experimental results, the corrections to the oblique parameters coming from the new fermionic fields must be very small.

The full chiral group of a TC-model depends on the TC gauge group and the representation at which the technifermions are implemented, and thus the number of Goldstone bosons, formed in the chiral symmetry breaking leading to EWSB, is specific for each TC-model. Three of the Goldstone bosons are eaten by the EW gauge boson but usually there are other Goldstone bosons that are left over. Some of these obtain small masses when the electroweak gauge couplings are turned on but some in general stay massless. The problem is that none of these massless or light Goldstone bosons have been observed in the experiments. Generating high enough masses for these states such that they might evade the mass limits set by present day experiments is one of the challenges set to TC-models.

Other problematic issue in TC models are the fermion masses. Indeed, when the usual scalar Higgs is removed from theory, also the Higgs-fermion Yukawa couplings are lost, and the mass terms for the fermions vanish. To overcome this problem a new interaction, the extended technicolor (ETC), is usually introduced. This new gauge interaction is added to combine the technifermions with the SM fermions, so that after the EWSB the SM fermions obtain their masses from the TC condensate by interacting with the quark condensate through exchange of the ETC gauge bosons. The fundamental energy scale for the ETC is assumed to be orders of magnitude higher than the TC and so in low energies below EW scale, where the ETC symmetry is broken, the interaction between the technicolor condensate and SM fermions can be viewed as an effective 4-point fermion interaction. That is, at low energies the ETC gauge boson interactions are considered to be a point like interactions described by the following non-renormalizable operators [54]:

$$\alpha_{ab}\frac{\bar{Q}\gamma_\mu T^a Q\bar{\psi}\gamma^\mu T^b\psi}{\Lambda^2_{ETC}}+\beta_{ab}\frac{\bar{Q}\gamma_\mu T^a Q\bar{Q}\gamma^\mu T^b Q}{\Lambda^2_{ETC}}+\gamma_{ab}\frac{\bar{\psi}\gamma_\mu T^a\psi\bar{\psi}\gamma^\mu T^b\psi}{\Lambda^2_{ETC}}\,. \qquad (3.1)$$

Here Q denotes the techniquarks and ψ the SM fermions, T^a's are the yet unspecified ETC generators and the coefficients α_{ab}, β_{ab} and γ_{ab} are parameters specific to the underlying ETC model. Phenomenologically the most important operators can be assorted from the above by Fierz rearrangement:

$$\alpha_{ab}\frac{\bar{Q}T^aQ\bar{\psi}T^b\psi}{\Lambda^2_{ETC}} + \beta_{ab}\frac{\bar{Q}T^aQ\bar{Q}T^bQ}{\Lambda^2_{ETC}} + \gamma_{ab}\frac{\bar{\psi}T^a\psi\bar{\psi}T^b\psi}{\Lambda^2_{ETC}} + \dots \tag{3.2}$$

After the techniquark condensation in low energies the first operator with a coefficient α_{ab} gives following masses to SM fermions:

$$m_f \approx \frac{g^2_{ETC}}{M^2_{ETC}} \left\langle \bar{Q}Q \right\rangle_{ETC}, \tag{3.3}$$

where g_{ETC} is the ETC running coupling constant evaluated at the Λ_{ETC}-scale. Also the TC condensate is calculated at ETC-scale and the M_{ETC} is the mass of the ETC gauge bosons after the ETC symmetry breaking. A realistic ETC-model should explain the mass hierarchy between the different families of SM fermions and also between quarks and leptons and in the end the mass differences within the weak doublets like electron vs. neutrino masses. Models which can produce hierarchies for the families have been studied in ref. [56] and more recently in [57]. The basic idea for generating the hierarchy within these models is fairly simple: Models have a large ETC group structure which sequentially breaks down to the TC gauge group $SU(N_{TC})$ at the TC scale. At each ETC symmetry breaking, a distinct condensate $\left\langle \bar{Q}Q \right\rangle_{ETC}$ is formed and since each condensate is formed in a different scale the mass hierarchies in the SM families are produced. The highest partial ETC breaking scale produces the lowest masses and the lowest ETC breaking scale the highest masses for the SM families. A general consideration of these models is beyond the scope of this thesis. However a naive estimate for the SM fermion mass can be obtained in the case of a QCD-like technicolor model by using the Eq. (3.3) and an approximation which states that in the ETC breaking scale (not specified here) the condensate scales as $\langle \bar{Q}Q \rangle_{ETC} \sim \langle \bar{Q}Q \rangle_{TC} \sim \Lambda^3_{TC}$. Further if only one weak doublet of technifermions is considered and if the interaction between the SM and TC fermions is mediated by an electroweak singlet ETC gauge boson which has a mass $M_{ETC} \sim g_{ETC}\Lambda_{ETC}$, the mass estimate becomes

$$m_f \sim \frac{\Lambda^3_{TC}}{\Lambda^2_{ETC}}. \tag{3.4}$$

Using this approximation and the assumption that $\Lambda_{TC} \approx 100$ GeV, an ETC scale $\Lambda_{ETC} \lesssim 1$ TeV is needed to obtain medium mass quark $m_{\text{charm}} \sim 1$ GeV. This seems reasonable, but getting the top quark mass $m_t \approx 100$ GeV right seems more problematic and gives a harder challenges to the TC and ETC model-building.

The operator with a coefficient β_{ab} in Eq. (3.2) gives rise to a masses for the pseudo-Goldstone bosons and for the techniaxions. The previously mentioned

problem concerning the light masses of these particles can thus be partially solved with the ETC interactions and even further alleviated in the context of the walking type TC-models, which are introduced in the following section. Obtaining heavy masses for these new mesons is not discussed further here; for a discussion see [54] and [55].

Finally the operator with a coefficient γ_{ab} in Eq. (3.2) produces the unwanted flavor changing neutral current (FCNC) processes. For example processes like $\mu \to \mu\bar{e}e, e\gamma$ may occur through an exchange of a heavy ETC gauge boson but such processes are forbidden by the experimental observations. Suppressing these flavor changing neutral currents is possible by increasing Λ_{ETC}-scale, as seen from the Eq. (3.2). However, when the experimental bounds are combined with naive ETC models the obtained limit is $\Lambda_{ETC} \gtrsim 10^3$TeV [58] which is in conflict with the estimate for the quark masses given below the Eq. (3.4). Indeed, with this FCNC limit the quark masses would be scaled down to $m_f \sim 100$MeV which is obviously a too low value. Also the FCNC problem is alleviated in the walking TC models to be considered next.

3.2.1 Walking TC

As discussed above, in the QCD-like TC models it is difficult to produce the heavy quark masses and suppress the flavor changing neutral currents at the same time. To get a better insight of these problems and to find a way to solve them one should consider the full TC dynamics. It is enlightening to study the scale evolution of the techniquark condensate since the quark and lepton masses are related to it. As was previously mentioned, the techniquark condensate is evaluated at the ETC-scale. Using the renormalization group methods one can estimate its value at the TC-scale, which is the relevant scale in light of the present day experiments. The condensate values at these two scales are related as [54];

$$\langle \bar{Q}Q \rangle_{ETC} = \exp\left(\int_{\Lambda_{TC}}^{\Lambda_{ETC}} d(\ln \mu) \gamma_m(\alpha(\mu)) \right) \langle \bar{Q}Q \rangle_{TC} \,, \tag{3.5}$$

where γ_m is the anomalous mass dimension and $\alpha(\mu)$ the running coupling evaluated at the scale μ. Now for a QCD-like TC dynamics the coupling constant is expected to scale as the QCD-running coupling $\alpha(\mu) \propto 1/\ln \mu$ in scales $\mu \gtrsim \Lambda_{TC}$, and the anomalous dimension is expected to behave as $\gamma_m \propto \alpha(\mu)$. With these approximations the integral in the Eq. (3.5) can be easily worked out and the values of the condensate at the two scales get related as:

$$\langle \bar{Q}Q \rangle_{ETC} \sim \left(\frac{\ln \Lambda_{ETC}}{\ln \Lambda_{TC}} \right)^{\gamma_m} \langle \bar{Q}Q \rangle_{TC} \,. \tag{3.6}$$

Thus the correction to the condensate given by the strong dynamics is only a power-logarithmic factor. This has only a small effect that can be ignored in the first approximation i.e. $\langle \bar{Q}Q \rangle_{ETC} \sim \langle \bar{Q}Q \rangle_{TC}$. This estimate, with

$\langle \bar{Q}Q \rangle_{TC} \sim \Lambda_{TC}^3$, was already used when the fermion masses were considered in Eq. (3.4). However, this scaling, and consequently the problem between obtaining the heavy quark masses and suppression of the flavor changing neutral currents can be alleviated with the 'walking' type strong dynamics. Indeed, if a model is considered where the coupling constant stays nearly a constant over the energy scales from Λ_{TC} to Λ_{ETC} (meaning that the coupling rather walks than runs to the UV fixed point), then the correction factor to the condensate becomes a power law. This kind of behavior of the coupling constant is possible if the theory has a near conformal fixed point. In this case the coupling $\alpha(\mu) \approx \alpha^*$ is approximatively constant, staying in the vicinity of the IR conformal fixed point α^* over the range $\Lambda_{TC} \lesssim \mu \lesssim \Lambda_{ETC}$. The anomalous dimension is evaluated at the apparent fixed point $\gamma_m(\alpha^*)$ [1] and the equation relating condensate at different scales becomes

$$\langle \bar{Q}Q \rangle_{ETC} \sim \left(\frac{\Lambda_{ETC}}{\Lambda_{TC}} \right)^{\gamma_m(\alpha^*)} \langle \bar{Q}Q \rangle_{TC} \,. \tag{3.7}$$

Using this estimate for the condensate with $\langle \bar{Q}Q \rangle_{TC} \sim \Lambda_{TC}^3$ and $M_{ETC} \sim g_{ETC}\Lambda_{ETC}$ as before, one can see that in walking TC models increasing the ETC-scale suppresses the FCNC as wanted while the SM fermion masses will not be reduced too dramatically as was in the case of naive QCD-like TC models. This scaling of the condensate helps increasing also the masses of the technimesons.

While walking behavior helps getting suitable SM quark masses, elevates the technimeson masses and helps to suppressing the FCNC, it does not necessarily make the model consistent with the EW precision data. Indeed, the EW measurements show that the oblique parameters S, T and U should be very small. Usually, in TC models, the reduction of the S-parameter is most challenging because S is sensitive to the number of new matter fields. For example the problem with the first realizations of the walking dynamics was that the matter fields were put into the fundamental representation of TC, whereby a large number of flavors was needed to produce the walking behavior. This however made the S-parameter too large and the model inconsistent with EW data. Thus in TC model building the theories with low number of matter fields and near conformal behavior are the ones of greatest interest.

In the end the evolution of the coupling, walking or running, depends on the gauge dynamics, the chosen TC gauge group and the representations at which the technifermions are implemented, because these factors define the form of the beta-function. Thus studying the phase structure of SU(N) gauge theories with matter fields in arbitrary representations as a function of the number of colors N and number of flavors N_f has been of particular interest in recent research (for a recent review see e.g. [55]). In its different phases the theory may be confined (QCD-like, running coupling), near conformal or conformal (walking or

[1] In the walking TC models the anomalous dimension is estimated to be $\gamma_m(\alpha^*) \simeq 1$ [54].

constant coupling) or the asymptotic freedom may be lost (QED-like coupling). The general study of phase structures of different theories helps to find the favorable TC models. However, finding plausible TC models is not the primary subject of this thesis and thus this subject will not be dwelled on further here. Instead particular minimal walking TC models, where a minimal number of new matter fields are implemented in higher dimension representations of TC group to produce the desired walking behavior will be considered next.

3.3 Minimal walking TC

The minimal walking technicolor (MWT) was introduced by Sannino and Tuominen [59]. This model has two techniflavors (quarks) in the two index symmetric (adjoint) representation of the SU(2) technicolor gauge group. Since the two index symmetric representation of SU(2) is real, the techniquarks can be combined in the following form, showing the global chiral SU(4) structure,

$$Q^a = \begin{pmatrix} U_L^a \\ D_L^a \\ -i\sigma_2 U_R^{*a} \\ -i\sigma_2 D_R^{*a} \end{pmatrix}, \tag{3.8}$$

where U and D represent the two new TC flavors and the upper index $a = 1, 2, 3$ is the technicolor index indicating the three dimensional adjoint representation. The left handed fields can be rearranged into three doublets $(U_L^a, D_L^a)^T$ of the $SU(2)_L$ weak interactions. The formation of techniquark condensate at $\sim \Lambda_{TC}$ breaks the global SU(4) group to SO(4) leading to the appearance of nine Goldstone bosons. Three of these will be eaten by the EW gauge bosons and the right mass ratios for the gauge bosons are guaranteed by the custodial SU(2) symmetry included in the SO(4). Procedure leaves out six quasi-Goldstone bosons which should receive masses from the ETC dynamics. These are expected to show up in the low energy spectrum of the theory and thus as a possible signal of the MWT in the Large Hadron Collider (LHC) experiments in CERN. Because the SU(2) adjoint representation is three dimensional there are only three new weak doublets and thus the model suffers from the global Witten anomaly [60]. To cure the anomaly a new heavy lepton family is introduced [59]:

$$L_L = \begin{pmatrix} E_L \\ N_L \end{pmatrix} \qquad E_R,\, N_R\,. \tag{3.9}$$

Here L_L is the left handed weak doublet constructed from the left handed 'electron' E_L and 'neutrino' N_L fields and the E_R and N_R are the corresponding right handed singlets. The gauge anomaly can be canceled with a generic hypercharge assignment

$$\begin{aligned} Y(Q_L) &= \tfrac{y}{2}\,, & Y(U_R, D_R) &= \left(\tfrac{y+1}{2}, \tfrac{y-1}{2}\right), \\ Y(L_L) &= -3\tfrac{y}{2}\,, & Y(E_R, N_R) &= \left(\tfrac{-3y+1}{2}, \tfrac{-3y-1}{2}\right), \end{aligned} \tag{3.10}$$

where y can be any real value. In these studies the SM-like convention $y = 1/3$ will be used throughout.

In ref. [59] it was shown that this model should be governed by a quasi-stable infrared fixed point (IRFP) and thus it is expected to have the walking-like behavior. This result is supported by the recent lattice data, see e.g. ref. [61]. Furthermore, the small number of technicolor matter fields keeps the S-parameter small, which is further reduced because of the new heavy leptons. In refs. [62] and [63] it was shown that the model is indeed consistent with the EW data and that, in contrast to the QCD-like or ordinary walking TC models, the MWT model can produce a light Higgs mass of $m_H \approx 90 - 150$ GeV.

To study the collider phenomenology and to overcome the problems concerning the fermion masses, an effective low energy theory of MWT was introduced in [64]. The effective theory accounts for the low energy spectrum of composite scalar, pseudoscalar, vector and pseudovector particles expected to rise from the underlying strongly interacting theory. As discussed previously, the fermion masses are usually generated by introducing another strongly interacting theory ETC (e.g. [57]). Yet another commonly used method to generate fermion masses is to introduce a new fundamental scalar sector to which the fermions are coupled (see e.g. [65] and [66]). In the effective MWT model [64] fermions were coupled to effective composite Higgs forming Yukawa-like couplings. In this approach the SM-like effective Higgs couplings parameterize the unknown form of the ETC theory and the model, as one may expect, looks effectively like the SM at low energies. The usual mixing patterns of the SM quarks and both Dirac and Majorana mass terms for the neutrinos can be obtained within the effective model.

The new heavy leptons and especially the cosmological implications of the new heavy neutrinos are the subject of real interest in this thesis. The existence of these states is natural in MWT model because they were necessary to remove the global Witten anomaly. Since these leptons have not been observed in colliders these particles are expected to be heavy, a natural scale in this case being the EW scale. In addition, the non-degeneracy of leptons is strongly favored in the MWT fits to EW precision data. Further, if there exists some symmetry (for example Z_2) that prevented the new neutrino from mixing with the SM fields and if this neutrino is lighter than the corresponding charged lepton (as is again favored by the EW data), the neutrino becomes an excellent candidate for the dark matter. The dark matter aspects of these neutrinos, in different mass scenarios, have been studied extensively in articles [I, II]. A summary and a generalized extension of these works will be presented in the next chapter. The related collider phenomenology of these heavy leptons has been studied in [67].

The MWT is a very interesting model for the EW symmetry breaking. It provides an EWSB dynamically without a fundamental Higgs. It overcomes the problems related to older QCD-like TC models and it is consistent with the present EW precision data, and it provides plausible dark matter candidates.

It thus provides a compelling alternative to supersymmetry. However, one appealing feature in the SUSY, contrast to MWT model described above, is that it provides the standard model coupling constant unification. Unification arises naturally in SUSY, albeit with the price of a dramatic increase of the number of degrees of freedom. Yet, only few of the new SUSY fields, the gauginos, are relevant for the unification. Thus the large number of new degrees of freedom (and the fact that the SUSY needs to be broken, because of the non-observation of light supersymmetric states,) lowers the beauty of the SUSY. Thus one might ask what needs to be added to the MWT to obtain the SM coupling constant unification as well? It turns out that only two additional Weyl fermions in suitable representations of the SM gauge groups are needed. This theory is considered in more detail below.

3.4 Minimal extension of the MWT

Extension of the MWT which produces unification of the SM coupling constants was proposed by Gudnason, Ryttov and Sannino in [68]. This model is the minimal extension of the SM which can potentially solve the three problems which were laid out in the beginning of this chapter; produce naturally EWSB, the dark matter and the gauge coupling unification. All this can be achieved by adding only three new Weyl fermions, which are TC singlets, to the MWT. Two of these Weyl fermions are need for the one loop unification; one in the adjoint representation of SU(3) QCD color and the other in the adjoint representation of SU(2) weak isospin. These degrees of freedom are in fact similar to the SUSY gauginos; the gluinos and the winos. Note that these two Weyl fermions are singlets under the other SM charges. To complete the partial symmetry within the 'gaugino'-sector, which seems natural and is motivated and required by the possible mass unification, also a third Weyl fermion associated with the hypercharge gauge interaction, the bino, is added to the system. This particle is expected to be a singlet under all SM and TC gauge interactions and its effects are felt only through the mass mixing. The mass mixing of the singlet with the neutral state of SU(2) adjoint triplet and the dark matter aspects of the corresponding mass eigenstates will be discussed in more detail in the next chapter.

Since already in the underlying MWT the techniquarks are in the two index symmetric representation of TC gauge group, adding new matter fields in higher dimensional representations in unifying model is quite natural. Yet adding matter fields in even higher than the two-index representations can easily spoil the asymptotic freedom of the theory [69]. For naturality i.e. avoiding the low energy fine tuning of the coupling constants, the asymptotic freedom of the theory is required. This essentially restricts the rank of representations to the ones discussed above.

A common feature in most unifying theories is that they generally predict

a proton decay. The unification scale is related to the proton lifetime and so the experiments which study the stability of the protons set a lower bound for the unification scale. Thereby to be a realistic unifying model this extension of the MWT needs to predict a high enough a unification scale. Finally also the unification of TC coupling constant with SM couplings can be speculated [68]. This issue does not alter the dark matter aspects which are the priority in this work and so the generalized unification will not be discussed further here.

3.4.1 Unification

The formal procedure for obtaining the SM coupling constant unification in the present minimally extended MWT model is the following: First the Higgs degrees of freedom are eliminated from the SM and replaced with the MWT degrees of freedom. The absence of Higgs and the existence of techniquarks and the new leptons will make the evolution of the weak and the hypercharge coupling constants differ from that of the SM. Next, the two new Weyl fermions, which are in the adjoint representations of color and weak isospin, are added; the former changes the running of QCD coupling and the latter further modifies the evolution of the weak coupling. The singlet bino does not effect to the running of the couplings at least at the one loop level. In the unifying theories, as it was shown in [70], only the particles not forming complete representations of the unifying group contribute to the unification. Of course all the particles coupled to some gauge group affect the running of the corresponding coupling constant, but the beta function coefficients arising from particles forming complete representations of the full unifying group cancel.

One could expect that also the TC interactions affect the running of the SM couplings, and indeed, in perturbation theory the TC coupling constant corrections to SM couplings appear at the two loop level. Moreover, one could argue that the perturbative evaluation of these TC corrections is not valid at low energies because of the strong dynamics. However, the lattice simulations of the MWT model [61] suggest the existence of an infrared fixed point at a fairly small coupling, which makes the use of perturbative theory reasonable. It turns out that the two loop TC contribution to the weak beta function is small, of the order of 10% when compared to the one loop result [III]. Further, going higher in energy, towards the unification scale, the TC coupling constant only decreases, whereby the running of the weak coupling is not expected to be substantially altered by the TC corrections.

One could also expect that the ETC interactions, either through some new strong dynamics or possibly via a new fundamental scalar related to fermion masses, could effect to evolution of the SM couplings. As discussed in the previous section the ignorance of the complete ETC model and thereby the ignorance of the generation of the fermion masses can be parameterized with an effective SM-like Higgs field. However, while the effective Higgs may be used to provide the fermion masses and to study the low energy phenomenology, it is not nec-

essarily reliable to use it to study the unification. The effective Higgs model is valid only up to some ETC-scale, which at least in the usual strongly interacting ETC models is much less than the unification scale, so that the contributions of the effective Higgs to the SM beta functions and thus to running of the couplings breaks down above the ETC-scale. Thus the contributions of the effective Higgs to the SM one loop beta functions are not reliable, and can be used at most as a suggestive estimate, up to the unification scale. The case is different if the ETC is expected to consist of a fundamental scalar, but then one may of course speculate about the sensibility of the reintroduction of the fundamental scalar into the theory. Anyhow, it would be reasonable to use some specific strong dynamics model to calculate the ETC corrections to the unification above the ETC-scale. In practice these corrections arise only at the two loop level. The crossover from the low energy effective ETC theory to the strongly interacting ETC theory gives uncertainty to the behavior of ETC coupling and thereby to the effects of the ETC to the SM beta functions. It is thus very difficult to estimate the effect of the undefined ETC-corrections to the unification and thus the ETC corrections are completely left out from the analysis. The precise unification analysis, in the present extended MWT model, is presented in article [III] which follows the analysis done in [68].

To conclude, the MWT and its minimal extension, discussed above are well motivated models for the dynamical electroweak symmetry breaking and possibly for the SM coupling constant unification. In addition they give rise to interesting dark matter candidates including a fourth family heavy neutrino and an SU(2) adjoint weyl fermion, and an extra SM singlet that can mix with either or both of the firstly mentioned fields. To study the dark matter nature of these particles, qualitatively concrete models need to be considered. Thereby a general model including the mass terms and the interactions for these particles will be specified next. In the model that will be introduced the particle densities can be calculated in different mass scenarios and the model parameter space can be constrained with the observational and experimental data.

Chapter 4

Dark matter model

The dark matter analysis done in articles [I], [II] and [III] is motivated and essentially based on the minimal walking technicolor model. The models start from the simplest MWT with a single heavy neutrino in ref. [I] and then extend to more general MWT with mixing heavy neutrinos in ref. [II]. Other favorable properties (gauge coupling unification) lead to an MWT model with adjoint particles and new dark matter particle candidates, which are studied in ref. [III]. In the following chapter the most general (DM) model in this framework, from which all the results in [I]- [III] can be obtained as limiting cases, will be presented. The particle spectrum of this model contains the left handed fourth family neutrino which makes the MWT model anomaly free, and a left handed neutral adjoint Weyl particle from the SU(2) adjoint triplet, which enables the SM gauge coupling unification, and a new right handed singlet. The singlet can be interpreted as a right handed sterile neutrino or just a new generic right handed singlet Weyl fermion. A new Z_2 symmetry is postulated to stabilize the dark matter particle arising from this scenario. This procedure is very similar to SUSY, where the WIMP is the lightest supersymmetric particle (LSP) in the mixture of the neutralinos, stabilized by the R-parity.

4.1 General model

The MWT and its unification extension contain several new particles: techniquarks, technigluons, 4^{th} family heavy leptons, SU(2) adjoint Weyl fermions and SU(3) adjoint Weyl fermions and the right handed singlet state postulated above, in addition to the speculative ETC sector. The neutral states contained in this set of states are potential dark matter candidates. However, the strongly interacting particles are not considered as primary DM candidates in the present study, and thereby the TC sector is not contemplated further here. Also the QCD-SU(3) adjoint Weyl fermions are assumed to be heavy and decoupled from the system. Thus the general dark matter sector considered here contains a 4^{th} family heavy neutrino, an SU(2) adjoint particle and a neutral singlet. The

relevant low energy Lagrange density for this model is

$$\mathcal{L}_{\rm GM} = \mathcal{L}_{\rm 4.f} + \mathcal{L}_{\rm Ad} + \mathcal{L}_{\rm SM-Higgs} + \mathcal{L}_{\rm Eff.Higgs} + \mathcal{L}_{\rm rest}\,, \tag{4.1}$$

where $\mathcal{L}_{\rm 4.f}$ denotes the $4^{\rm th}$ generation lepton family part, $\mathcal{L}_{\rm Ad}$ the SU(2) adjoint Weyl fermions, $\mathcal{L}_{\rm SM-Higgs}$ the SM without the fundamental Higgs field, $\mathcal{L}_{\rm Eff.Higgs}$ the low energy effective Higgs part and finally $\mathcal{L}_{\rm rest}$ denotes the TC-sector, SU(3) adjoint Weyl fermions and possible other ETC terms which do not have important role in the dark matter analysis. The possible right handed singlet state is included in $\mathcal{L}_{\rm Ad}$.

This chapter is organized as follows. First the Lagrangians introduced in Eq. (4.1) and especially the gauge interactions of the fourth family heavy leptons and the SU(2) adjoint Weyl fermions are studied, and their possible mass generation mechanisms are introduced. Second a general mixing pattern between the fourth family neutrino, the neutral adjoint particle and neutral right handed singlet is established and the effects of the mixing to gauge interactions and to effective Higgs interactions are presented. Then the significance of the Majorana phases relating to the dark matter mass positivity is discussed, using 2×2 mass mixing as an example. Finally the model results and the constraints arising from the DM search experiments will be discussed.

4.2 Weak currents

4.2.1 Weak currents for heavy leptons

To make the complete model SU(2) gauge anomaly free, the hypercharges for the new TC quarks and for the new leptons are chosen similarly as for SM quarks and leptons, as was already noted in connection with Eq. (3.10). Let E denote the new charged lepton and N the new heavy neutrino so that $L_L = (N_L E_L)^T$ is the left handed doublet and E_R is the charged right handed singlet. The hypercharges that produce the SM like charges are $Y(E_L) = Y(N_L) = -1/2$ and $Y(E_R) = -1$. The kinetic and gauge interaction terms in the Lagrangian density for the fourth family leptons can be written similarly as for the SM leptons. In the charge basis this Lagrange density is

$$\begin{aligned} \mathcal{L}_{\rm 4.f} &= i\bar{L_L}\not{\partial}\, L_L + i\bar{E_R}\not{\partial}\, E_R + \mathcal{L}_{\rm 4.f,H} \\ &\quad + \mathcal{L}_{\rm W} + \mathcal{L}_{\rm Z} + \mathcal{L}_{\rm EM}\,, \end{aligned} \tag{4.2}$$

where the weak and electromagnetic currents are

$$\begin{aligned} \mathcal{L}_{\rm W} &= \frac{g}{\sqrt{2}}(W^-_\mu \bar{E}_L\gamma^\mu N_L + W^+_\mu \bar{N}_L\gamma^\mu E_L), \\ \mathcal{L}_{\rm Z} &= \frac{g}{\cos\theta_W} Z_\mu \Big(\bar{N}_L\gamma^\mu(\tfrac{1}{2})N_L + + \bar{E}_L\gamma^\mu(-\tfrac{1}{2} + \sin^2\theta_W)E_L \\ &\qquad + \bar{E}_R\gamma^\mu(\sin^2\theta_W)E_R \Big)\,, \\ \mathcal{L}_{\rm EM} &= -eA_\mu \bar{E}\gamma^\mu E\,, \end{aligned} \tag{4.3}$$

and the θ_W is the Weinberg angle. The difference in Eq. (4.2) when compared to the Lagrangian of the SM leptons arise from the mass-Lagrangian included in $\mathcal{L}_{4.\mathrm{f,H}}$, which will be introduced explicitly in Sec. 4.3 below.

4.2.2 Weak currents for the SU(2) adjoint Weyl fermions

The second ingredient in the general DM model are the left handed SU(2) adjoint Weyl fermions. These have a major role in the unification of SM gauge coupling constants, which was considered in in Sec. 3.4.1. Also a right handed singlet Weyl fermion is introduced, which does not affect the SM gauge unfication but is crucial for the dark matter scenario. The Lagrangian density of the Weyl fermions is then

$$\mathcal{L}_{\mathrm{Ad}} = i\omega^\dagger \bar{\sigma}^\mu D_\mu \omega + i\beta\sigma^\mu \partial_\mu \beta^\dagger + \mathcal{L}_{\mathrm{Ad,H}}\,, \tag{4.4}$$

where $\omega = (w^1, w^3, w^3)$ is the left-handed triplet, $\beta^\dagger$ the right-handed singlet and $\bar{\sigma}^\mu \equiv (1, -\vec{\sigma})$ and $\sigma^\mu \equiv (1, \vec{\sigma})$ with $\vec{\sigma}$ presenting a vector constructed from the Pauli matrices. The covariant derivative D_μ in the component form is

$$D_\mu^{ac} = \partial_\mu \delta^{ac} + g\epsilon^{abc} A_\mu^b\,, \tag{4.5}$$

where $[T^a]_{bc} = -i\epsilon^{abc}$ are the $\mathrm{SU}_L(2)$ generators in the adjoint representation. That is, the field ω transforms as a triplet under $\mathrm{SU}_L(2)$ and is a singlet under hypercharge. The field $\beta^\dagger$ is singlet under all SM gauge groups.

Next these 2-component fields will be written in a more familiar 4-component form, as charged Dirac and neutral Majorana fields. This makes the calculation of the annihilation cross sections straightforward since the usual Dirac matrix machinery is then available. We start by finding the charged states. Since the charge operator is $Q = T^3 + Y$ and the ω field is a hypercharge singlet the eigenstates of diagonal weak isospin T^3 generator are also the charge eigenstates. In the adjoint representation the diagonalizing matrix of T^3 is

$$D = \begin{pmatrix} \frac{1}{\sqrt{2}} & 0 & \frac{1}{\sqrt{2}} \\ \frac{i}{\sqrt{2}} & 0 & -\frac{i}{\sqrt{2}} \\ 0 & 1 & 0 \end{pmatrix}. \tag{4.6}$$

After the diagonalization[1] the eigenstates are

$$w^\pm = \frac{1}{\sqrt{2}}(w^1 \mp iw^2), \quad w^0 = w^3 \tag{4.7}$$

which have the electromagnetic charge ± 1 and 0, as the notation suggests. Using these fields one easily finds the kinetic terms

$$i\omega^\dagger \bar{\sigma}^\mu \partial_\mu \omega = iw^{+\dagger} \bar{\sigma}^\mu \partial_\mu w^+ + iw^{-\dagger} \bar{\sigma}^\mu \partial_\mu w^- + iw^{0\dagger} \bar{\sigma}^\mu \partial_\mu w^0\,. \tag{4.8}$$

[1]Diagonalization is done by $\omega^\dagger D D^\dagger T^3 D D^\dagger \omega$ where the eigenstates are $D^\dagger \omega$

Similarly the gauge interaction term becomes

$$\mathcal{L}_{\text{gauge}} = ig\epsilon^{abc} w^{a\dagger} \bar{\sigma}^{\mu} A^{b}_{\mu} w^{c} \tag{4.9}$$

$$= g \begin{pmatrix} w^{+\dagger} w^{0\dagger} w^{-\dagger} \end{pmatrix} \bar{\sigma}^{\mu} \begin{pmatrix} W^{3}_{\mu} & -W^{+}_{\mu} & 0 \\ -W^{-}_{\mu} & 0 & W^{+}_{\mu} \\ 0 & W^{-}_{\mu} & -W^{3}_{\mu} \end{pmatrix} \begin{pmatrix} w^{+} \\ w^{0} \\ w^{-} \end{pmatrix} \tag{4.10}$$

where the charged gauge bosons are defined as usual: $W^{\pm}_{\mu} = (A^{1}_{\mu} \mp i A^{2}_{\mu})/\sqrt{2}$. All expressions can then be transformed from the Weyl notation to the 4-dimensional Dirac notation by defining Dirac spinors carrying negative and positive charges:

$$w^{-}_{D} = \begin{pmatrix} w^{-}_{\alpha} \\ (w^{+})^{\dagger\dot{\alpha}} \end{pmatrix}, \quad w^{+}_{D} = \begin{pmatrix} w^{+}_{\alpha} \\ (w^{-})^{\dagger\dot{\alpha}} \end{pmatrix}. \tag{4.11}$$

Similarly the neutral 4-component Majorana spinors can be defined:

$$w^{0}_{M} = \begin{pmatrix} w^{0}_{\alpha} \\ (w^{0})^{\dagger\dot{\alpha}} \end{pmatrix}, \quad \beta_{M} = \begin{pmatrix} \beta_{\alpha} \\ \beta^{\dagger\dot{\alpha}} \end{pmatrix}. \tag{4.12}$$

These satisfy $(w^{-}_{D})^{c} = w^{+}_{D}$, $(w^{0}_{M})^{c} = w^{0}_{M}$ and $(\beta_{M})^{c} = \beta_{M}$. Since only one of the charged spinors can be treated as an independent degree of freedom, everything can be written using only w^{0}_{M}, β_{M} and either of the charged Dirac-spinors $w^{\pm}_{D}$. Setting $w_{D} \equiv w^{-}_{D}$ the Lagrangian (4.4) can be written as

$$\mathcal{L}_{\text{Ad}} = i\bar{w}_{D} \not{\partial} w_{D} + i\bar{w}_{M} \not{\partial} w_{M} + i\bar{\beta}_{M} \not{\partial} \beta_{M} + \mathcal{L}_{\text{Ad,H}}$$
$$+ g \left(W^{+}_{\mu} \overline{w}^{0}_{M} \gamma^{\mu} w_{D} + W^{-}_{\mu} \overline{w}_{D} \gamma^{\mu} w^{0}_{M} - W^{3}_{\mu} \overline{w}_{D} \gamma^{\mu} w_{D} \right). \tag{4.13}$$

The field β_{M} does not couple to electroweak gauge fields but may mix with the neutral adjoint state through the mass terms represented by $\mathcal{L}_{\text{Ad,H}}$ in Eq. (4.17). The desired charged and neutral currents can be read from Eq. (4.13):

$$\mathcal{L}_{W} = g(W^{+}_{\mu} \overline{w}^{0}_{M} \gamma^{\mu} w_{D} + W^{-}_{\mu} \overline{w}_{D} \gamma^{\mu} w^{0}_{M}), \tag{4.14}$$
$$\mathcal{L}_{Z} = g \cos\theta_{W} Z_{\mu} \overline{w}_{D} \gamma^{\mu} w_{D},$$
$$\mathcal{L}_{A} = e A_{\mu} \overline{w}_{D} \gamma^{\mu} w_{D}.$$

It is important to note that the field w^{0}_{M} does not couple to the neutral gauge boson Z_{μ}. Therefore, if the DM particle is dominantly a $w^{0}_{M} - \beta_{M}$-mixture only the charged current processes will have significant role in the dark matter analysis.

4.3 Effective mass terms

To obtain the mass terms for the fourth family leptons, SU(2) adjoint particles and for the singlet, an effective Higgs doublet is introduced to the model. This procedure is practical and natural since the more complete ultraviolet ETC-theory presumably manifests itself as an effective Higgs-like model in low energies, as previously discussed in Sec. 3.3.

4.3.1 Mass terms for heavy leptons

For the effective Higgs couplings to the 4$^{\rm th}$ family leptons and to charge neutral singlet field β_M, the following gauge invariant effective interactions, including dimension five operators, are introduced:

$$\begin{aligned}\mathcal{L}_{\rm 4.f,H} &= y_E \bar{L}_L H E_R + \text{h.c.} \\ &+ C_D \bar{L}_L \tilde{H} \beta_R + \text{h.c.} \\ &+ \frac{C_L}{\Lambda}(\bar{L}^c \tilde{H})(\tilde{H}^T L) + \text{h.c.}\,. \end{aligned} \tag{4.15}$$

Here $\tilde{H} = i\tau^2 H^*$ and y_E, C_D and C_L are some dimensionless coupling constants, and Λ is a suppression factor related to the more complete ultraviolet theory, expected to generate the full flavor structure emerging above the electroweak scale. The first term is the usual SM-like Yukawa term which gives the Dirac mass term for the charged leptons. The second term is an SM-like Yukawa coupling of the left handed neutrino and the singlet which generates a Dirac like mass term that mixes the neutrino and the singlet states. This coupling could be considered to give the left-right Dirac mass term if the right handed singlet is interpreted as a right handed sterile neutrino[2]. The last term is a non-renormalizable dimension five operator which produce the left handed Majorana mass terms for the neutrinos.

Note that the interactions in Eq. (4.15), as well as the other terms in Eqs. (4.2) and (4.13), are invariant under Z_2 symmetry transformation, in which $E \to -E$, $N \to -N$, $\beta \to -\beta$ and $w \to -w$. Such interactions, Eqs. (4.15), (4.2) and (4.13) as well as the following Eq. (4.17) below do not connect the adjoint fermions to ordinary matter and hence do not endanger the stability of the DM candidate.

After the spontaneous symmetry breaking (SSB) where $\sqrt{2}H \to (0, v+h)^T$ Eq. (4.15) becomes

$$\begin{aligned}\mathcal{L}_{\rm 4.f,H} &\overset{\rm SSB}{\to} m_D^E \overline{E}_D E_D \left(1 + \frac{h}{v}\right) \\ &+ \frac{m_D^{\beta N}}{2}(\overline{\beta}_R N_L + \overline{\beta}_L N_R)\left(1 + \frac{h}{v}\right) + \text{h.c.} \\ &+ \frac{M_L^N}{2}\overline{N}_M N_M \left(1 + \frac{h}{v}\right)^2, \end{aligned} \tag{4.16}$$

where the masses are $m_E \equiv y_E v/\sqrt{2}$, $m_D^{\beta N} \equiv C_D v/\sqrt{2}$ and $M_L^N \equiv C_L v^2/\Lambda$ and v is the vacuum expectation value (VEV) of the effective Higgs field h. Note that $(N_M)^c = N_M$. Here and in the following the shorthand 4-component notations $N_L \equiv N_{ML} = (N_\alpha, 0)^T$, $N_R \equiv N_{MR} = (0, N^{\dagger\dot{\alpha}})^T$, $w_L^0 \equiv w_{ML}^0 = (w_\alpha^0, 0)^T$ and $\beta_R \equiv \beta_{MR} = (0, \beta^{\dagger\dot{\alpha}})^T$ are used.

[2]Note that the pure right-handed Majorana mass term for the singlet is given, in connection with the mass terms of SU(2) adjoint Weyl fermions, below.

4.3.2 Mass terms for the SU(2) adjoint Weyl fermions

For the Higgs couplings to the SU(2) adjoint particles, to 4^{th} family neutrino and to singlet β_M with mixings, the following effective interactions, which include dimension five operators and also respect the Z_2-symmetry, are considered:

$$\begin{aligned}\mathcal{L}_{\text{Ad,H}} &= \frac{\lambda_L}{\Lambda}H^\dagger\omega\omega H + \text{h.c.} \\ &+ y_w\tilde{H}^T\omega L_L + \text{h.c.} \\ &+ \frac{\lambda_D}{\Lambda}\beta H^\dagger\omega H + \text{h.c.} \\ &+ \frac{\lambda_R}{\Lambda}\beta\beta H^\dagger H + \text{h.c}\,, \end{aligned} \tag{4.17}$$

where $\omega \equiv \omega^a\tau^a$ and $\tau^a = \sigma^a/2$ in terms of the Pauli matrices. The suppressing scale Λ is as in Eq. (4.15). When $\sqrt{2}H \to (0, v+h)^T$, Eq. (4.17), written in the 4-component notation, becomes

$$\begin{aligned}\mathcal{L}_{\text{Ad,H}} &\overset{\text{SSB}}{\to} (M_L^w\overline{w}_D w_D + \frac{M_L^w}{2}\overline{w}_M^0 w_M^0)\left(1+\frac{h}{v}\right)^2 \\ &+ \frac{m_D^{wN}}{2}(\overline{w}_R^0 N_L + \overline{w}_L^0 N_R)\left(1+\frac{h}{v}\right) + \text{h.c.} \\ &+ \frac{m_D^{\beta w}}{2}(\overline{\beta}_R w_L^0 + \overline{\beta}_L w_R^0)\left(1+\frac{h}{v}\right)^2 + \text{h.c.} \\ &+ \frac{M_R^\beta}{2}\overline{\beta}_M\beta_M\left(1+\frac{h}{v}\right)^2, \end{aligned} \tag{4.18}$$

where $M_L^w \equiv \lambda_L v^2/4\Lambda$ simultaneously gives the mass of the charged w_D field and the Majorana mass of the state w_M^0 constructed from the adjoint triplet. Dirac like mixing mass terms are $m_D^{wN} \equiv y_w v/2\sqrt{2}$ and $m_D^{\beta w} \equiv \lambda_D v^2/2\Lambda$. Finally $M_R \equiv \lambda_R v^2/\Lambda$ is a right-handed Majorana mass for the β_M-field.

In the above scenario the singlet field β_M interacts with the SM-like Higgs state through the term in the last line of the Eq. (4.17) (and Eq. (4.18)). Alternatively the β_M field can receive its mass in a dynamical symmetry breaking from the VEV of a new weak SU(2) singlet field S, which can plausibly emerge from a more complete extended technicolor theory. The gauge- and Z_2 symmetric interaction Lagrangian for $\beta^\dagger$ and S is

$$\mathcal{L}_{\beta S} = y_R S\beta\beta + \text{h.c.} \overset{SSB}{\to} \frac{M_R}{2}\overline{\beta}_M\beta_M\left(1+\frac{s}{v_s}\right), \tag{4.19}$$

where, after the symmetry breaking in which $\sqrt{2}S \to v_s + s$, the mass $M_R \equiv \sqrt{2}y_R v_s$ with v_s being the VEV of the singlet S. In the dark matter density calculations the β_M-mass generating scenario using the last line of Eq. (4.18) will be refered as scenario I and the one using Eq. (4.19) as scenario II. The change from the scenario I to the scenario II can be done by replacing the last

line in Eqs. (4.17) and (4.18) with Eq. (4.19). Of course a combination of the two scenarios could also be studied, but this case is not considered in this thesis.

Finally note that similar to [71], gauge invariance allows us to write a Yukawa couplings

$$\begin{aligned} & y_w^i H^T(i\tau^2)\omega L_i + y_\beta^i H^T(i\tau^2)\beta L_i + \text{h.c.} \\ = \; & -\frac{v+h}{\sqrt{2}}[y_w^i(\sqrt{2}w^+ e_i + w^0\nu_i) + y_\beta^i \beta\nu_i] + \text{h.c.} \end{aligned} \tag{4.20}$$

where the L_i is generation i SM lepton doublet. These kind of terms would endanger the stability of the dark matter particle since they couple SM fields to the adjoint ω fields so that the ω fields and thus the possible dark matter particle could decay to lighter SM particles. However, these terms are forbidden by the postulated Z_2 symmetry as the SM model fields are thought to be singlets under Z_2.

4.4 Mass mixing

In the following section the mass terms of the neutral particles N_M, w_M^0 and β_M, introduced in the previous section, will be collected to form a general mixing mass matrix, and the many consequences of the diagonalization of this mass matrix will be considered, such as different mixing scenarios, the mass eigenvalue positivity, gauge couplings and effective Higgs couplings in the mass eigenbasis and the Majorana nature of the dark matter particles in the context of Feynman rules.

4.4.1 General mass mixing

The general 3×3 mass matrix of the new neutral Majorana particles can easily be formed by collecting all but the first (involving charged fields) mass terms from the equations (4.16) and (4.18). The resulting matrix in the four component notation reads

$$\mathcal{L}_{\text{mass}} = \frac{1}{2}\begin{pmatrix} \overline{N_R} & \overline{w_R^0} & \overline{\beta_R} \end{pmatrix} \begin{pmatrix} M_L^N & m_D^{wN} & m_D^{\beta N} \\ m_D^{wN} & M_L^w & m_D^{\beta w} \\ m_D^{\beta N} & m_D^{\beta w} & M_R^\beta \end{pmatrix} \begin{pmatrix} N_L \\ w_L^0 \\ \beta_L \end{pmatrix} + \text{h.c.} \tag{4.21}$$

This mass matrix induces an analogous mixing pattern to that described by the Pontecorvo-Maki-Nakagawa-Sakata (PMNS) matrix in the 3×3 light neutrino mixing. This mixing matrix differs from the usual Cabibbo-Kobayashi-Maskawa (CKM) matrix in the quark mixing in that it includes extra Majorana phases. Note that in the present case the mixing matrix appearing in charged weak currents is a retangular 2×3-matrix. To clarify this issue let us briefly discuss about the general $N \times N$ mass mixing.

In general a complex $N \times N$ mass matrix (M') has $2N^2$ independent real parameters and it can be diagonalized by a biunitary transformation: $V_L^\dagger M' V_R = M$, where the two diagonalizing unitary matrices $V_L^\dagger$ and V_R have N^2 independent real parameters each. Furthermore the N^2 independent real parameters of the general diagonalizing $N \times N$ unitary matrix can be divided into $N(N-1)/2$ mixing angles and to $N(N+1)/2$ phases. Yet not all the phases are physically observable. The physical effects of the mixing are seen in the weak gauge interactions and except these weak current terms the Lagrangian is invariant under global phase transformations of the fields. Thus a number of the phases in the generic diagonalizing matrix (which appears in the total mixing matrix in the weak currents) can be eliminated by this rephasing of the fields.

In the studied case $N = 3$ but actually the mixing matrix seen in the weak currents is not precisely unitary, but rectangular 2×3 matrix since in this case we have only two charged Dirac fields E_D and w_D to accompany with the three neutral fields, in contrast to the three (flavors of) charged fields in the usual lepton or quark mixing. Still, the treatment of the mass matrix diagonalization is similar to that of three Majorana neutrino 3×3 mixing. Indeed, the diagonalizing unitary matrices in these cases are the same. The retangular mixing matrix, which appears in the weak currents, is then formed by taking just the two upper rows of the 3×3 diagonalizing (mixing) matrix. These issues are considered in more detailed in [72].

It turns out that in this case there are 3 mixing angles and 5 phases of which two phases can be eliminated by making suitable global phase transformations for the charged fields. Note that the neutral fields cannot be rephased since the mass Lagrangian contains Majorana mass terms which are not invariant under these phase rotations. So the final unitary matrix which diagonalizes the Eq. (4.21) mass matrix has 3 mixing angles and 3 physical phases which can be divided using the usual terminology into one Dirac phase and two Majorana phases. Standard parametrization for this matrix is:

$$U_{\rm mix} = U_D U_M = \tag{4.22}$$

$$\begin{pmatrix} c_{12}c_{13} & s_{12}c_{13} & s_{13}e^{-i\delta_{13}} \\ -s_{12}c_{23} - c_{12}s_{23}s_{13}e^{i\delta_{13}} & c_{12}c_{23} - s_{12}s_{23}s_{13}e^{i\delta_{13}} & s_{23}c_{13} \\ s_{12}s_{23} - c_{12}c_{23}s_{13}e^{i\delta_{13}} & -c_{12}s_{23} - s_{12}c_{23}s_{13}e^{i\delta_{13}} & c_{23}c_{13} \end{pmatrix} \begin{pmatrix} 1 & 0 & 0 \\ 0 & e^{i\lambda_2} & 0 \\ 0 & 0 & e^{i\lambda_3} \end{pmatrix}$$

Here U_D matrix is the usual CKM matrix and the diagonal U_M contains the additional Majorana phases. Further, $c_{ij} \equiv \cos\vartheta_{ij}$ and $s_{ij} \equiv \sin\vartheta_{ij}$ where the three mixing angles $0 \leq \vartheta_{ij} \leq \pi/2$ refer to the rotations in i,j-plane and the CP-violating Dirac and Majorana phases are restricted to $0 \leq \delta_{13} \leq 2\pi$, $0 \leq \lambda_i \leq 2\pi$ respectively.

Further reduction of the mixing matrix can be done only by making further approximations on the mass matrix. For example the assumption that the mass terms are real drops all the phases out of the diagonalizing matrix. This is

the scenario which will be considered in this thesis for simplicity. Still, the mass eigenvalues might be negative, and to overcome this problem an additional diagonal phase matrix ρ is introduced. These phases are related to the Majorana phases of the Majorana particles and they contribute to the definition of the intrinsic CP-parities of the mass eigenstates.

There are two possible ways of dealing with these ρ-phases. Either the diagonal phase matrix is divided to two taking a root of the original matrix, so that the phases will be integrated to the diagonalizing unitary matrix. In this case the field operators are independent of the phases but the phases will appear explicitly in the vertex Feynman rules. Another possibility is that the phases are substituted to the field operators whence they become the Majorana phases of the particles. An approach similar to the former case, restricted to the 2×2 mass matrix, was studied in [67]. In this work the latter option is used and will be explained in more detail.

To calculate the dark matter density from the Lee-Weinberg equation the dark matter annihilation cross sections are needed. To define these cross sections, the weak currents and the effective Higgs couplings need to be rewritten in mass eigenbasis and thus the diagonalization of the mass matrix and the relations between the mass and flavor states need to be specified in detail. These will be done next.

4.4.2 Mixing and couplings

The diagonalization of the mass matrix $M_{\rm mass}$ presented in Eq. (4.21) can be done by using $U_{\rm mix}$ from the Eq. (4.22). Since Majorana mass matrix is symmetric $M_{\rm mass} = M_{\rm mass}^T$ it can be diagonalized with transformation $U_{\rm mix}^T M_{\rm mass} U_{\rm mix} = m$, where the mass eigenvalues are $m_i \geq 0$.

Yet, if the mass matrix is expected to be real; $M_{\rm mass} = M_{\rm mass}^*$, the matrix $U_{\rm mix}$ further reduces to an orthogonal matrix O_D which is just the U_D from Eq. (4.22) without the Dirac phase factor. So the general real and symmetric mass matrix can be diagonalized as

$$O_D^T M_{\rm mass} O_D = m' \equiv \text{diag.}(\lambda_1', \lambda_2', \lambda_3'), \tag{4.23}$$

where λ_i' is the i'th mass eigenvalue, which still can be positive or negative. To ensure that the physical masses are positive, a diagonal phase matrix ρ is implemented, so that $m' = \rho m$ and the ρ_i:s are chosen such that masses m_i are always positive. These ρ_i's are the phases mentioned in the end of the last section and they will have important effects on the results as will be clarified in the following sections.

Now, by using the relations $O_D^\dagger O_D = O_D^T O_D = 1$, $\rho\rho^\dagger = 1$ and the notation

$\Omega_L \equiv (N_L\, w_L^0\, \beta_L)^T$, Eq. (4.21) can be written in the form

$$\begin{aligned}
\mathcal{L}_{\rm mass} &= \frac{1}{2}\overline{\Omega_R} M_{\rm mass}\Omega_L + \frac{1}{2}\overline{\Omega_L} M_{\rm mass}\Omega_R \\
&= \frac{1}{2}\overline{\Omega_R} O_D \rho\rho^\dagger O_D^T M_{\rm mass} O_D O_D^T \Omega_L \\
&+ \frac{1}{2}\overline{\Omega_L} O_D O_D^T M_{\rm mass} O_D \rho^\dagger \rho O_D^T \Omega_R \\
&= \frac{1}{2}\overline{\chi} m \chi\,, \qquad (4.24)
\end{aligned}$$

where the m is the diagonal mass matrix with positive mass eigenvalues and the mass eigenstates are defined as

$$\chi = \chi_L + \chi_R \equiv O_D^T \Omega_L + \rho O_D^T \Omega_R\,, \qquad (4.25)$$

which obey the Majorana condition $\chi_i^c = \rho_i \chi_i$. From Eq. 4.25 can be immediately inverted

$$\Omega_L = O_D \chi_L\,, \quad \Omega_R = O_D \rho \chi_R\,. \qquad (4.26)$$

Now the weak currents and the effective Higgs couplings can be written in the mass eigenbasis. Still, at this point one should notice that the phase factors ρ_i appear in the mass eigenstates, or inversely in flavor states, and thus will influence the gauge and Higgs couplings when these are represented in mass eigenbasis. But before proceeding to these couplings let us comment the relations for solving the mass eigenvalues using the mixing angles.

To specify the mass eigenvalues and the mixing angles the mass terms in the original mass matrix need to be specified. Finding the relations and particularly the inverse relations, giving the original mass matrix in terms of the eigenmasses, mixing angles and ρ-phases in the case of a general 3×3 mass matrix is intricate and thus the explicit relations will not be given here. In general the diagonalization is easily done numerically. However, the relations for eigenvalues and mixing angles to the original mass parameters will be presented in an example case of 2×2 mixing in Sec. 4.4.4.

Mixing and gauge couplings

Using the Eqs. (4.3), (4.14) and (4.26) the weak currents of the heavy leptons and of the SU(2) adjoint fermions in the mass eigenbasis become

$$\mathcal{L}_{\rm 4.f}^{\rm W} = \frac{g}{\sqrt{2}}[W_\mu^-(O_{11}\bar{E_L}\gamma^\mu\chi_{1L} + O_{12}\bar{E_L}\gamma^\mu\chi_{2L} + O_{13}\bar{E_L}\gamma^\mu\chi_{3L}) + \text{h.c.}]\,, \qquad (4.27)$$

$$\begin{aligned}
\mathcal{L}_{\rm 4.f}^{\rm Z} &= \frac{g}{2\cos\theta_W} Z_\mu[(O_{11})^2\bar{\chi_{1L}}\gamma^\mu\chi_{1L} + (O_{12})^2\bar{\chi_{2L}}\gamma^\mu\chi_{2L} + (O_{13})^2\bar{\chi_{3L}}\gamma^\mu\chi_{3L} + \\
&\quad O_{12}O_{11}\bar{\chi_2}(A_{21} + B_{21}\gamma^5)\gamma^\mu\chi_1 + O_{13}O_{11}\bar{\chi_3}(A_{31} + B_{31}\gamma^5)\gamma^\mu\chi_1 + \\
&\quad O_{13}O_{12}\bar{\chi_3}(A_{32} + B_{32}\gamma^5)\gamma^\mu\chi_2]\,, \qquad (4.28)
\end{aligned}$$

$$\begin{aligned}
\mathcal{L}_{\rm Ad}^{\rm W} &= gW_\mu^-[O_{21}\overline{w}_D\gamma^\mu(A_1 - B_1\gamma^5)\chi_1 + O_{22}\overline{w}_D\gamma^\mu(A_2 - B_2\gamma^5)\chi_2 + \\
&\quad O_{23}\overline{w}_D\gamma^\mu(A_3 - B_3\gamma^5)\chi_3] + \text{h.c.}\,, \qquad (4.29)
\end{aligned}$$

where the real matrix elements O_{ij} are the elements of U_D from Eq. (4.22) without the complex phase factors; $\exp(\pm i\delta_{13}) \to 1$, and

$$A_{ij} \equiv \frac{1}{2}(1-\rho_{ij}) \quad \text{and} \quad B_{ij} \equiv \frac{1}{2}(1+\rho_{ij}), \tag{4.30}$$

$$A_i \equiv \frac{1}{2}(1+\rho_i) \quad \text{and} \quad B_i \equiv \frac{1}{2}(1-\rho_i), \tag{4.31}$$

where $\rho_{ij} \equiv \rho_i\rho_j$. It should be emphasized that w_M^0 does not couple to the Z-boson and thus if the WIMP is dominantly $w_M^0 - \beta_M$ mixture the charged current will control the dark matter abundance.

Mixing and Higgs couplings

Further, using the equations (4.16), (4.17), (4.19) and (4.26) the couplings to effective Higgs can be reduced to

$$\begin{aligned}\mathcal{L}_{h\chi} = -\frac{g}{2M_W}\Big[&C_{11}^h h\bar{\chi_1}\chi_1 + C_{22}^h h\bar{\chi_2}\chi_2 + C_{33}^h h\bar{\chi_3}\chi_3 + \\ &\frac{C_{11}^{h^2}}{v}h^2\bar{\chi_1}\chi_1 + \frac{C_{22}^{h^2}}{v}h^2\bar{\chi_2}\chi_2 + \frac{C_{33}^{h^2}}{v}h^2\bar{\chi_3}\chi_3 + \\ &C_{12}^h h\bar{\chi_1}(B_{12} - A_{12}\gamma^5)\chi_2 + C_{13}^h h\bar{\chi_1}(B_{13} - A_{13}\gamma^5)\chi_3 + \\ &C_{23}^h h\bar{\chi_2}(B_{23} - A_{23}\gamma^5)\chi_3\Big] + \dots ,\end{aligned} \tag{4.32}$$

where M_W is $W^\pm$-boson mass, $v = 2M_W/g$ is the vacuum expectation value of the Higgs boson and the projection factors A_{ij} and B_{ij} are as defined in Eq.(4.30). The mixing angle, mass and phase factor dependent coefficients C_{ij} are specified in Table 4.1. The dots refer to the terms which do not affect the tree level matrix element calculations and are thus left out from the expression.

The equations (4.27)-(4.32) include most of the information needed to calculate the annihilation matrix elements. Yet the Majorana nature of the particles and the phases ρ_i, as previously mentioned, will have further consequences for the calculations. These will be considered in the following section. From Eqs. (4.27)-(4.32) it can be seen, that the interaction terms get coupled with mixing angle dependent factors (O_{ij}) in the mass eigenbasis. These factors, when small, are responsible of the reduction of the coupling strengths which subsequently causes the decrease of the annihilation cross sections. This suppression of the annihilation cross sections from the standard weak interaction strength enables the increase of the dark matter density as explained in the end of the Chapter 2.

4.4.3 Accounting for the mixing phases

The matrix element calculations are much more laborious with general mixing Majorana fields than with the usual Dirac fields, in part because general Feynman rules are lacking in the case of mixing Majorana fields. The ρ-phases affect

	Scenario I	Scenario II
C^h_{11}	$m_1(\frac{1}{2} - \frac{m_D^{\beta N}}{m_1}\rho_1 O_{11}O_{31})$	$m_1(\frac{1}{2} - \frac{m_D^{\beta N}}{m_1}\rho_1 O_{11}O_{31} - \frac{M_R^\beta}{m_1}\rho_1 O_{31}^2)$
C^h_{22}	$m_2(\frac{1}{2} - \frac{m_D^{\beta N}}{m_2}\rho_2 O_{12}O_{32})$	$m_2(\frac{1}{2} - \frac{m_D^{\beta N}}{m_2}\rho_2 O_{12}O_{32} - \frac{M_R^\beta}{m_2}\rho_2 O_{32}^2)$
C^h_{33}	$m_3(\frac{1}{2} - \frac{m_D^{\beta N}}{m_3}\rho_3 O_{13}O_{33})$	$m_3(\frac{1}{2} - \frac{m_D^{\beta N}}{m_3}\rho_3 O_{13}O_{33} - \frac{M_R^\beta}{m_3}\rho_3 O_{33}^2)$
$C^{h^2}_{11}$	C^h_{11}	$m_1(\frac{1}{2} - \frac{m_D^{\beta N}}{m_1}\rho_1 O_{11}O_{31} - \frac{1}{2}\frac{M_R^\beta}{m_1}\rho_1 O_{31}^2)$
$C^{h^2}_{22}$	C^h_{22}	$m_2(\frac{1}{2} - \frac{m_D^{\beta N}}{m_2}\rho_2 O_{12}O_{32} - \frac{1}{2}\frac{M_R^\beta}{m_2}\rho_2 O_{32}^2)$
$C^{h^2}_{33}$	C^h_{33}	$m_3(\frac{1}{2} - \frac{m_D^{\beta N}}{m_3}\rho_3 O_{13}O_{33} - \frac{1}{2}\frac{M_R^\beta}{m_3}\rho_3 O_{33}^2)$
C^h_{12}	$m_1[-\frac{m_D^{\beta N}}{m_1}\rho_1(O_{11}O_{32} + O_{12}O_{31})]$	$m_1[-\frac{m_D^{\beta N}}{m_1}\rho_1(O_{11}O_{32} + O_{12}O_{31}) - 2\frac{M_R^\beta}{m_1}\rho_1 O_{31}O_{32}]$
C^h_{13}	$m_1[-\frac{m_D^{\beta N}}{m_1}\rho_1(O_{11}O_{33} + O_{13}O_{31})]$	$m_1[-\frac{m_D^{\beta N}}{m_1}\rho_1(O_{11}O_{33} + O_{13}O_{31}) - 2\frac{M_R^\beta}{m_1}\rho_1 O_{31}O_{33}]$
C^h_{23}	$m_2[-\frac{m_D^{\beta N}}{m_2}\rho_2(O_{12}O_{33} + O_{13}O_{32})]$	$m_2[-\frac{m_D^{\beta N}}{m_2}\rho_2(O_{12}O_{33} + O_{13}O_{32}) - 2\frac{M_R^\beta}{m_2}\rho_2 O_{32}O_{33}]$

Table 4.1: Shown are the coefficients of the different type of composite Higgs - χ -interactions from the both β-mass generating scenarios.

non-trivially the calculations and the number of possible contractions increases dramatically because of the Majorana nature of the particles. To clarify these issues, some explicit Feynman rules for mixing Majorana fields with non-trivial phase matrix will now be given, including the in- and out-state and propagator Feynman rules. Also the general features of the ρ-phases will be discussed. Further, in the Appendix an explicit example of a detailed calculation of a matrix element is represented.

Feynman rules. According to definition (4.25) $\chi^c = \rho\chi$. This means that the phases ρ_i must appear in the Majorana field operators, which now become

$$\chi_i = \sum_h \int \frac{\mathrm{d}^3k}{(2\pi)^3}\left[\hat{a}_{h\mathbf{k}i}u_{hi}(k)e^{-ikx} + \rho_i\hat{a}^\dagger_{h\mathbf{k}i}v_{hi}(k)e^{ikx}\right], \tag{4.33}$$

where the sum is over the helicities h. This operator gives rise to the following nontrivial contractions in the momentum space Feynman rules:

$$\begin{aligned} \underbrace{\chi_i\hat{a}^\dagger_{h\mathbf{p}i}} &= u_{hi}(p) \qquad \text{and} \qquad \underbrace{\bar{\chi}_i\hat{a}^\dagger_{h\mathbf{p}i}} = \rho_i^*\bar{v}_{hi}(p) \\ \underbrace{\hat{a}_{h\mathbf{p}i}\chi_i} &= \rho_i v_{hi}(p) \qquad \text{and} \qquad \underbrace{\hat{a}_{h\mathbf{p}i}\bar{\chi}_i} = \bar{u}_{hi}(p)\,. \end{aligned} \tag{4.34}$$

Only the first two of these will be needed in computations because in all processes these WIMPs appear in the initial state only. In Majorana case one also has four different internal contractions, or propagators:

$$\begin{aligned} \underbrace{\chi_i(x)\bar{\chi}_i(y)} &= iS_i(x-y) \\ \underbrace{\chi_i(x)\chi_i(y)} &= iS_i(x-y)(-\rho_i C) \\ \underbrace{\bar{\chi}_i(x)\bar{\chi}_i(y)} &= (\rho_i^* C)iS_i(x-y) \\ \underbrace{\bar{\chi}_i(x)\chi_i(y)} &= (\rho_i^* C)iS_i(x-y)(-\rho_i C)\,, \end{aligned} \tag{4.35}$$

where $iS_i(x-y)$ is the standard Dirac propagator for the mass eigenstate i, and C is the usual charge conjugation matrix. Note that above Feynman rules can be used for particles with general $N \times N$ Majorana mixing as long as the mass matrix is real and symmetric. In that case $i = 1, \ldots, N$.

ρ-phases. Of course the original mass matrix defines uniquely the mass eigenvalues and their signs and thus especially the phases ρ_i. As seen previously these phases appear in several relations and thus appear to have consequences for the model predictions. Indeed, accounting for the mixing phases is relevant. Although the individual phases ρ_i are not physical observables, the relative phases $\rho_i\rho_j = \rho_{ij}$ are[3]. They show up explicitly in the calculations, as in weak gauge- and Higgs couplings, and they define physically distinct regions in the model parameter space. Although these phases are thus relevant, their consequences have not been appreciated in the literature before. To demonstrate the effects of these phases an explicit example is considered in next section.

One way of exploring the physical parameter space of the model is by using directly the physical mass and mixing angle values in the calculations. But in this case the relations between the physical parameters and the original Lagrange parameters is not always clear and physically different cases can easily be lost. The control of phases can be very difficult in this case. A second and more straightforward way is to make a Monte Carlo analysis for the Lagrange parameters. From every given parameter set the physical parameters can be solved and then the suitable physical parameter space of the model can be constructed by excluding those parameter regions which do not produce right dark matter abundance or do not satisfy experimental constrains following from collider or dark matter search experiments. The former case is considered in articles [II] and [III] and the latter method is more suitable to be used in the general 3×3 mixing model.

Instead of going deeper into the consequences of the phase matrix ρ and the diagonalization of the general 3×3 mass matrix, let us consider simpler mass scenarios which can be obtained from the 3×3 in certain limits. These examples are easier to deal with and yet they include the additional ρ phase matrix so that the implications of these phases can be studied explicitly. These are also the mass mixing patterns that appear in articles [II] and [III].

4.4.4 Example: 2×2 mass mixing

Within this example the mass mixing patterns appearing in articles [I]- [III] will be constructed. There are three different cases to be studied. The first article [I] considers the most trivial mass scenario were the dark matter particle has either a pure left handed Majorana or a pure Dirac mass term. This analysis will be left last. The articles [II]- [III] consider 2×2 mixing. In what follows

[3]In general $N \times N$ mixing there are $N-1$ physically distinct relative phases ρ_{ij}. This can be seen for example by noting that general $N \times N$ Majorana mixing includes the Majorana phase matrix with $N-1$ phases which can be rendered to form the total ρ-phase matrix.

the other member in the 2×2 mixing is always the singlet β and the mixing is named by the representation in which the other state is assembled under the weak interaction.

2×2 Doublet mixing

The article [II] considers a general 2×2 heavy neutrino DM mixing. The studied 2×2 mixing scenario can be constructed form Eq. (4.21) by setting certain mass terms to zero so that the mass term becomes:

$$\mathcal{L}_{\rm mass} = \frac{1}{2} \left(\begin{array}{ccc} \overline{N_R} & \overline{w_R^0} & \overline{\beta_R} \end{array} \right) \left(\begin{array}{ccc} M_L^N & 0 & m_D^{\beta N} \\ 0 & M_L^w & 0 \\ m_D^{\beta N} & 0 & M_R^\beta \end{array} \right) \left(\begin{array}{c} N_L \\ w_L^0 \\ \beta_L \end{array} \right) + \text{h.c.} \qquad (4.36)$$

When the β is considered as a four component Majorana neutrino constructed from the two component right handed sterile neutrino and if $M_L^w \gg M_L^N, M_R^\beta, m_D^{\beta N}$ the consequences of the mass mixing are equivivalent to the scenario studied in [II]. In this case the very heavy w^0 field is decoupled from the mixing lighter neutrino system. Still w^0 can be part of the total model and enable the unification of the SM coupling constants.

Note that the elimination of the certain mass terms can also be considered from the mixing matrix point of view just as a loss of certain mixings. In the above case this would mean that $m_D^{wN}, m_D^{\beta w} \to 0$ is equivivalent to $\vartheta_{12}, \vartheta_{23} \to 0$. Remembering that the original mass parameters are chosen to be real, this indicates that the phases are zero ($\delta_{13} = \lambda_1 = \lambda_2 = 0$) and so the following mixing matrix is obtained

$$U_{\rm mix,2} = U_{D,2} = \left(\begin{array}{ccc} c_{13} & 0 & s_{13} \\ 0 & 1 & 0 \\ -s_{13} & 0 & c_{13} \end{array} \right) . \qquad (4.37)$$

From this matrix the usual 2×2 diagonalizing orthogonal matrix O_D can be read from the corners.

To summarize, the 2×2 effective mass and the diagonalizing matrices in the present case are

$$M_{\rm mass} = \left(\begin{array}{cc} M_L^N & m_D^{\beta N} \\ m_D^{\beta N} & M_R^\beta \end{array} \right) , \; O_{\rm D} = \left(\begin{array}{cc} \cos\theta & \sin\theta \\ -\sin\theta & \cos\theta, \end{array} \right) , \qquad (4.38)$$

where the mixing angle $\theta \equiv \vartheta_{13}$ [4]. Now using the notation $\Omega_L \equiv (N_L\,, \beta_L)^T$ and the $M_{\rm mass}$ above the (N, β)-part of the Eq. (4.36) can be written in the form

$$\mathcal{L}_{\rm mass} = \frac{1}{2}(\overline{\Omega_R} M_{\rm mass} \Omega_L + \overline{\Omega_L} M_{\rm mass} \Omega_R) = \frac{1}{2} \overline{\chi} m \chi \,, \qquad (4.39)$$

[4]Note that in the following a notation $\chi \equiv (\chi_1\,, \chi_2)^T$ for the mass eigenstates are adopted in the reduced system. More correctly this should be $\chi \equiv (\chi_1\,, \chi_3)^T$. Similarly when the 2×2 mass and the mixing matrices etc. are considered the elements such as $O_{D,12}$ should be understood as $U_{D,13}$ from Eq. (4.37). This is relevant if one considers the weak and Higgs couplings. However the new notation is adopted because it is used in papers [II] and [III]. Similar notation will also be used in the adjoint mixing case consider below.

where the diagonal mass matrix is $m = \mathrm{diag}(m_1, m_2)$ with positive physical mass eigenvalues. The mass eigenstates $\chi \equiv (\chi_1\,, \chi_2)^T$, which obey the Majorana condition $\chi_i^c = \rho_i \chi_i$, are defined as

$$\chi = \chi_L + \chi_R \equiv O_D^T \Omega_L + \rho O_D^T \Omega_R\,, \tag{4.40}$$

where the diagonalizing orthogonal matrix O_{D} is of the form Eq. (4.38) and the associated mixing angle obeys the relation

$$\tan 2\theta = \frac{2m_D}{M_R - M_L}\,. \tag{4.41}$$

Also a new phase matrix $\rho = \mathrm{diag}(\rho_1, \rho_2)$ is introduced to ensure that the physical masses $m_{1,2}$ are positively definite. Indeed, the eigenvalues of the mass matrix M_{mass} in Eq. (4.38) are easily found to be

$$\lambda_\pm = \frac{1}{2}(M_L^N + M_R^\beta \pm \sqrt{(M_L^N - M_R^\beta)^2 + 4(m_D^{\beta N})^2})\,, \tag{4.42}$$

but these eigenvalues can be positive or negative depending on the signs and the relative magnitudes of the M_L^N, M_R^β and $m_D^{\beta N}$. Yet by choosing the phases as $\rho_\pm \equiv \mathrm{sgn}(\lambda_\pm)$ the physical masses will always stay positive $m_\pm = \rho_\pm \lambda_\pm = |\lambda_\pm|$ as required. For the dark matter calculations it will be convenient to express everything in terms of the physical mass eigenvalues $m_1 > m_2$ and the mixing angle $\sin\theta$ instead of the Lagrangian parameters M_L, M_R and m_D. While working with physical parameters has obvious advantages, the downside is that the connection between the physical and the Lagrangian parameters is not always straightforward as already mentioned in the previous sections and will be illustrated in the following.

Accounting for the mixing phases

Now the role of the phase-rotation matrix ρ and the the structure of the parameter space of the model will be discussed in detail.

In Fig. 4.1 shown is the parameter space along a plane of some nonzero value of m_D. Now suppose first that $M_R + M_L \geq 0$. Then the eigenvalue λ_+ (4.42) is always positive and larger than $|\lambda_-|$. Further choose to denote by χ_1 the heavier state, so that $\rho_1 \equiv \rho_+ = 1$ and so the WIMP is always associated with χ_2 with the mass $m_2 = m_-$. The sign of $\rho_2 = \rho_-$ is defined by the ratio of m_D^2 and $M_L M_R$: $\rho_2 = -1$ if $m_D^2 > M_L M_R$, and otherwise $\rho_2 = +1$. As previously mentioned the individual phases are not observable, but the relative phase corresponding to the product of the two is:

$$\rho_1 \rho_2 = \rho_+ \rho_- \equiv \rho_{12}\,. \tag{4.43}$$

In particular this phase will show up explicitly in the various couplings of the mass eigenstates. The situation with respect to the product phase is again

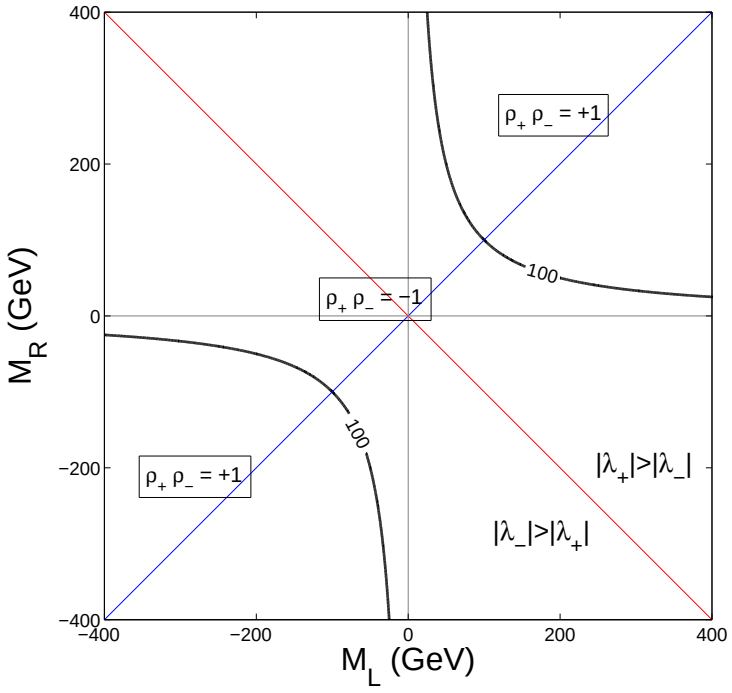

Figure 4.1: Shown is a constant-m_D slice of the mass parameter space, which is divided into physically disjoint regions by the sign of the effective phase $\rho_+\rho_-$. The physical parameters are invariant under the mirroring symmetry with respect to the line $M_R = -M_L$.

illustrated in Fig. 4.1: $\rho_+\rho_-$ is positive in the upper right corner separated by the black solid line and negative elsewhere in the region $M_R + M_L \geq 0$. From Eq. (4.41) is seen that $\tan 2\theta$ becomes infinite along the the line $M_L = M_R$, corresponding to a maximal mixing $|\theta| \equiv \pi/4$. The mixing angle is defined to be zero in the limit $M_R - M_L \gg |m_D|$, whereby $0 \leq |\theta| \leq \pi/4$ below and $\pi/4 \leq |\theta| \leq \pi/2$ above the line of maximal mixing. The sign of the mixing angle is determined by the sign of m_D. Physically, in the region below the line of maximal mixing, the WIMP is predominantly a sterile right chiral state while in the region above the line it is predominantly a left chiral state with ordinary weak interaction strength. It is thus clear that the area of most interest in this case is the rightmost quadrant bounded by the diagonal lines in the phase space in Fig. 4.1. Now consider the case $M_R + M_L \leq 0$. In this area λ_- is always negative and $|\lambda_-| > |\lambda_+|$. Thus, in this region the heavier state (which is always chosen to be labeled with N_1) has to be associated with N_-, while the WIMP is always the now lighter $N_2 \equiv N_+$. Here is always $\rho_1 = \rho_- = -1$ while the sign $\rho_1 = \rho_+$ again depends on the relative magnitude of $M_L M_R$ and m_D^2; the resulting division to distinct areas according to the sign of $\rho_{12} = \rho_-\rho_+$ is again shown in Fig. 4.1. There is an obvious symmetry in the phase space about the reflection along the line $M_L + M_R = 0$. Indeed, all that happens in this reflection is that the eigenvalues $\lambda_\pm$ and their associated eigenstates exchange roles, but all physical parameters θ, m_1, m_2 and ρ_{12} remain invariant. That is, the reflection corresponds to a mere relabeling $1 \leftrightarrow 2$ as the two regions can be mapped to each others by a redefinition of the phases of the states. Thus the region $M_R + M_L \geq 0$ is considered from now on. Nevertheless, for each triplet of physical mass and mixing parameters m_1, m_2 and θ the original parameter space contains two physically distinct solutions labeled by the relative phase ρ_{12}. In what follows, the results will be given always for both possibilities.

This subsection is concluded by noting that all the typical special cases are contained within the $\rho_{12} = -1$ portion of the parameter space: the pure left- or right-handed Majorana states correspond to $M_R = 0$ and $M_L = 0$ axes in the plane $m_D = 0$, respectively, while the $M_L = 0$ and $M_R = 0$ planes for nonzero m_D correspond to usual seesaw scenarios. Finally the Dirac limit corresponding to the axis $M_L = M_R = 0$ is also contained only in the $\rho_{12} = -1$ domain. It is perhaps due to this reason that the other domain with $\rho_{12} = +1$ has so far gone unnoticed in the literature.

Mass mixing and couplings

The WIMP couplings to weak gauge bosons and to the effective Higgs boson now follows from equations (4.27)-(4.32), when the mixing limits specified at the beginning of this section are taken. They naturally reduce exactly to the couplings represented in the article [II] in Sec. 2.3. Using these interactions the annihilation cross sections can be computed.

2×2 Adjoint particle mixing

Also the mixing matrix studied in article [III] can be obtained by a similar treatment as above. In this case by setting $m_D^{wN}, m_D^{\beta N} \to 0$ which coincide with $\vartheta_{12}, \vartheta_{13} \to 0$ (and again requiring the phases to be zero) the mass matrix and the mixing matrix becomes

$$M_{\rm mass} = \begin{pmatrix} M_L^N & 0 & 0 \\ 0 & M_L^w & m_D^{\beta w} \\ 0 & m_D^{\beta w} & M_R^\beta \end{pmatrix}, \; U_{\rm mix,3} = \begin{pmatrix} 1 & 0 & 0 \\ 0 & c_{23} & s_{23} \\ 0 & -s_{23} & c_{23} \end{pmatrix}. \qquad (4.44)$$

The resulting 2×2 mixing pattern arises when $M_L^N \gg M_L^w, M_R^\beta, m_D^{\beta w}$, and the mixing matrices are of the same form as in doublet (neutrino) mixing case and thus the accounting for the mixing phases are similar. Yet the couplings to gauge bosons and to effective Higgs boson are not the same. Instead, taking the mixing limits specified above, the equations (4.27)-(4.32) reduce to couplings studied in article [III] in Sec. II.D, which are different from the doublet mixing case.

Pure Dirac/Majorana mass terms

Finally the pure Dirac and pure left handed Majorana neutrino cases are considered. In the general 3×3 mass matrix all but $m_D^{\beta N}$ or M_L^N mass terms are now set to zero (or if considering that the adjoint state and the singlet state are present then assuming that M_L^ω and M_R^β are very large). In both cases no mixing angle dependence nor ρ-phase dependence appear in couplings since there is no mass mixing. In this case the heavy neutrinos are SM-like neutrinos, with pure Dirac or pure left handed Majorana mass terms, with standard weak interactions and standard (effective) Higgs interactions.

Since no mixing angle dependence exists the annihilation cross sections are not suppressed from the standard weak scale. As discussed in the Sec. 2.3.2 the standard weak scale annihilation cross section is not suitable to produce the correct dark matter density if standard radiation driven expansion is considered. This is because the too large cross section lets the annihilation of the particles proceed for too long, leading to a too large reduction of the particle density before the freeze-out. Thus to obtain the correct dark matter density this model needs a quintessence mechanism or something equivalent to boost the early universe expansion so that the freeze-out may occur earlier to allow the particle abundance to freeze in an acceptable level. This model, including quintessence, was studied in article [I], but the model is now essentially ruled out by the direct cryogenic DM search results as shown by the XENON10 collaboration in [52].

4.5 Results

Here a brief summary of the results presented in articles [II] and [III] will be given.

The relic DM density is in general dependent of the WIMP mass, the mixing angle(s), phases ρ_{ij}, the Higgs mass and the β-mass scenario. Also the mass(es) of the charged state(s) $(E_D, \omega_D^{\pm})$ and of the other neutral state(s) (χ_i) affect the final density of the lightest stable DM particle. However, these are less important parameters because these masses appear only in propagators in a sub-class of graphs in the annihilation cross section matrix elements. The mass hierarchies may be limited by experimental constrains such as the EW precision data. These aspects are considered in some detail in the Sec. 4.6. For further details see articles [I]- [III].

Doublet mixing results

Given the annihilation cross sections following from the results given in Secs. 4.4.2, 4.4.3, and 4.4.4 and Eq. (2.38), the density parameter values for the mixing 4^{th} family heavy neutrino dark matter can be solved from the Lee-Weinberg equation (2.41) together with the Eq. (2.44). The favorable constant density parameter Ω_N contours as a function of the WIMP mass and mixing angle are given in Figs. 4.2 and 4.3 in the different β-mass scenarios, ρ-phases and with different Higgs masses. The Ω_N values shown with thick solid and dashed contours are the ones consistent with the present DM density constraints given by the current WMAP results. In figures also plotted are the exclusion regions following from the LEP data (yellow areas) and the XENON10 results [52] (red areas) and moreover from the upcoming XENON100 updates (red lines). These constraints are discussed in more detail in Sec. 4.6. In conclusion the model gives correct dark matter density for a wide range of parameters but the cryogenic dark matter search experiments have started to constrain the parameters in an interesting way, and the model may be either verified or ruled out already by the XENON100-1T upgrades.

The form of the density parameter contours shown as a function of WIMP mass and mixing angle in Figs. 4.2 and 4.3 basically reflect the inverse cross section as a function of WIMP mass. The first dip (peak) in the contours (cross section) follows from the WIMP annihilation to the fermionic final states through the Z-boson exchange, so that as the cross section gets bigger in the Z-pole, the mixing angle needs to be suppressed to obtain the correct density. The second general characteristic seen in the contours is the opening of the W-boson final state channel in WIMP mass $\sim$80 GeV (Until this WIMP mass region the fermion final states define the final WIMP density). When the W-boson final state channel opens the cross section increases again and so the mixing angle needs to be decreased to set the correct DM density. This overall effect is partially disguised by the Higgs exchange and the Higgs pole, which results in

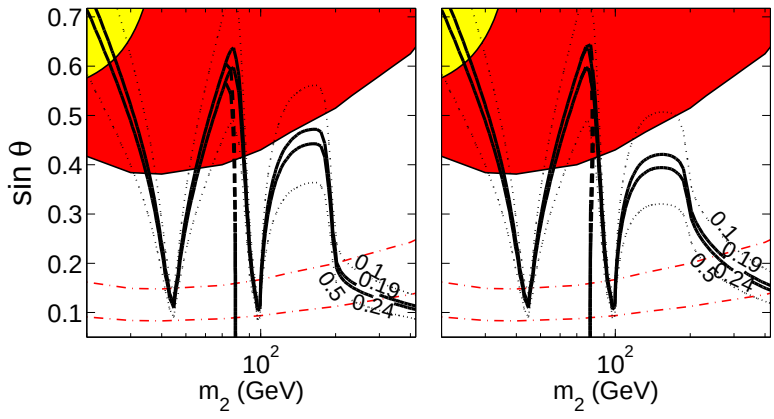

Figure 4.2: Shown are the constant Ω_N contours as a function of the mass and the mixing angle. The area between the contours with Ω_N =0.19 and 0.24 is consistent with the WMAP results for the dark matter density. In both panels $m_H = 200$ GeV was used. Thick solid lines correspond to the mass scenario II and thick dashed lines to the mass scenario I. In left panel $\rho_{12} = +1$ and in right panel $\rho_{12} = -1$. Thin dotted contours show further contours for the scenario II. The yellow (light shaded) area is excluded by the LEP limits and the red (dark shaded) area is excluded by the XENON10 [52] limits. The red dash-dotted lines show the predicted sensitivity of the XENON100 (upper line) and XENON100 update (lower line) as given in ref. [76].

the second dip in the contours. The last drop after second peak in the contours follows from the opening of the Higgs boson final state channel, which once again increases the cross section whereby the mixing angle needs to get further suppressed to obtain the correct density. Note that in the Fig. 4.3 this effect is not seen since the parameter space is only shown up to $m_{\rm WIMP} = 420$GeV which is less than the $m_H = 500$GeV at which point the new Higgs channel opens.

Adjoint mixing results

Similarly to the doublet case, the adjoint DM results are given in Figs. 4.4 and 4.5 as favorable density parameter constant contours in the plane of adjoint WIMP mass and mixing angle again in different mass scenarios, ρ-phase cases and with different Higgs masses. The DM density parameter values shown with thick solid and dashed contours are again the ones consistent with the current WMAP results. Also plotted are the exclusion regions following from LEP data (red lines) and the projected LHC data (green lines). These constraint curves are discussed in more detail in Sec. 4.6. Different curves correspond to different ratios for the neutral state masses, the lighter of which is the WIMP. Thick solid lines correspond to the ratio $A \equiv m_1/m_2 = 2$ which is used also in the density

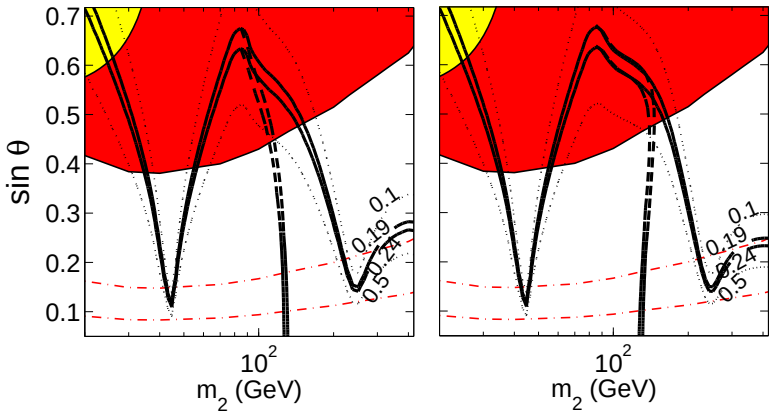

Figure 4.3: Same as in figure 4.3, but now for $m_H = 500$ GeV.

contour calculations. The dashed and dash-dotted lines corresponding to cases $A = 4$ and 1.5, respectively, show the trend that the bigger the mass hierarchy the weaker the constraint. The blue horizontal lines give the limits above which the charged adjoint particle is lighter than the neutral state: $m_D^{\omega} < m_{\mathrm{WIMP}}$. That area is excluded because in this case the dark matter particle would be charged. Once again the thick solid, dashed and dash-dotted lines correspond to mass hierarchies for the neutral states defined by $A = 2$, 4 and 1.5 respectively. Also in this case the conclusion is that the model gives correct dark matter density within a rather large parameter space and that collider experiments can constrain the model parameter space quite efficiently and that the model may be either verified or ruled out either by the LHC or in the upcoming XENON100-1T experiments (discussed in the next section).

Also in this case a few words should be said about the characteristics of the density parameter contours shown in Figs. 4.4 and 4.5. The clearest difference to the profiles in the previous doublet mixing case follows from the lack of WIMP-Z-boson coupling in the present scenario. Indeed, in these figures there is no Z-pole dip in the contours; the only dip visible here comes from the Higgs pole. Further, the suitable parameter space of the WIMP mass start only from the region where the channel to the W-boson final states opens. Basically the entire contour curve shape is determined by the W-boson final state and H-boson effects in the cross section. So to obtain the correct density value the mixing angle needs to be suppressed to compensate the increase of the cross section as a function of the WIMP mass which follows from the opening of the W-boson final state channel. Small corrections to this picture follow from the contributions to the cross section when the Z-boson and H-boson final states open up.

A final note to the results: as discussed in the end of the Chapter 2 the

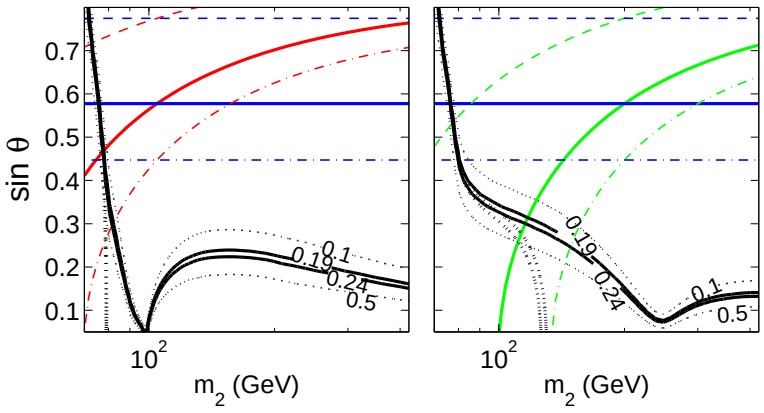

Figure 4.4: Shown are the constant Ω_χ contours as a function of WIMP mass and the mixing angle $\sin\theta$ with $\rho_{12} = -1$. Scenario I is shown by thick black dotted lines and scenario II by thick solid black and thin dotted lines. In left picture Higgs-boson mass is 200 GeV and in right picture 500 GeV. The area between the thick lines is favored by the WMAP results for dark matter density. Area to the left from thick red curve in the left panel is excluded by the LEP limit $m_{w_D} < 104.5$ GeV, assuming $m_1/m_2 \equiv A \geq 2$. The dash and dash-dotted lines shown the same limit assuming that $A = 4$ and $A = 1.5$ respectively. Similar (green) curves on the right panel show these constraints assuming an improved limit $m_{w_D} < 200$ GeV. The (blue) horizontal lines are the upper limits for the $\sin\theta$ coming from the requirement that $m_2 < m_{w_D}$, where the thick solid, thin dashed and thin dash-dotted lines again correspond to the cases $A = 2$, 4 and 1.5 respectively.

dynamical dark energy can have an effect to the cosmic WIMP density. This scenario could be considered in both of the above neutrino and adjoint particle dark matter cases. However, the effect to the results of, say the quintessence caused kination would be that the suitable density contours would rise in all figures shown. This is because the increased expansion rate lowers the need to suppress the cross section and thus the mixing angle would be bigger for a given target dark matter density. Of course this would result in the acceptable values moving into the zone excluded by the observations. Thus the effects of quintessence type expansion seem to actually be undesirable for these models. However, seen the other way around the effect of the quintessence could be to enlarge the allowed parameter space of the model, essentially to the entire region between the contour with $\Omega \approx 0.214$ and the current exclusion regions this can be easily visualized in all the results shown in Figs. 4.2, 4.3, 4.2 and 4.3.

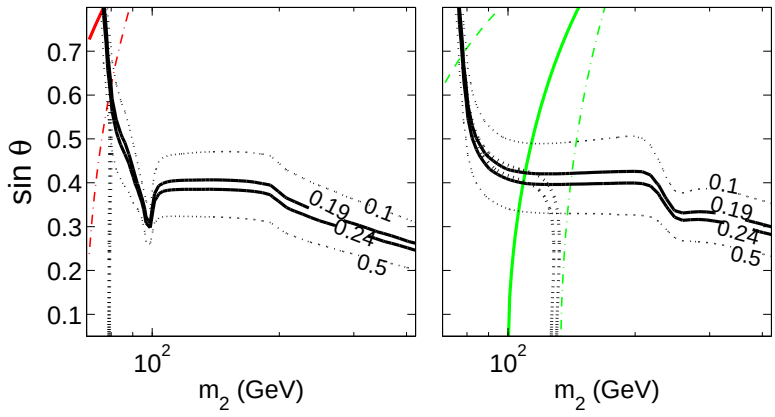

Figure 4.5: Same as in Figure 4.4 but for $\rho_{12} = +1$.

4.6 Constraints

Finally the dark matter models will be confronted with the experimental and observational data. Although no direct verification of the dark matter particles exists yet, several experiments efficiently constrain the parameter spaces of different dark matter models, as was already shown in the section above. In the following the most relevant experimental constraints for the studied dark matter model will be discussed in more detail.

4.6.1 LEP limits

The first limits to the model parameter space follow from the Large Electon Positron (LEP) collider data. The data can be used in two ways to constrain the model.

The first limits come from the measurements of the Z-boson decay width into invisible/neutral channel[5] [73, 74]. The measured value for the decay width into neutral particles almost exactly coincides with the decay width predicted by the three light SM neutrinos. A small deviation in the decay widths, allowed within the experimental errors, can be considered to be a non-standard origin arising from the model studied here. Naturally, these constraints apply only if the WIMP couples to the Z-boson. Since the fourth family neurtino has such a coupling, a WIMP which is predominantly an $N_L - \beta$ mixture can be constrained with this method. However, since the neutral SU(2) adjoint state is not coupled to Z-boson a WIMP which is dominantly a $\omega_0 - \beta$ mixture is not constrained by the Z-boson decay width data. Thus, depending on the relative N_L/ω_0 composition in the general WIMP, considered here, the model may or may not get a substantial limits from the Z-decay width.

[5] An accurate description how to make these constraints is given in [II] in Sec. 4.1.

The second constraint follows from the non-observation of the new heavy charged particles in LEP. Essentially the mass of the new charged particles is constrained to be more than half of the maximum collision energy in the CM-frame reached in the LEP experiment. This limit, however, only affects the charged lepton mass. It does not directly limit the heavy doublet neutrino because the new charged lepton and the neutrino masses are not necessarily coupled. However, the doublet neutrino, as a component of the WIMP, is expected to be lighter than the charged partner. The situation is different for the WIMP containing a nonzero fraction of ω. Indeed, since the ω_0 belongs to ω-triplet, the electrically charged states of which form the charged Dirac particle, the original mass parameters of the ω_0 and $\omega_D^{\pm}$ states are related, as seen from Eq. (4.18). Thus limiting the charged state masses one limits also the ω_0 mass term which, when a dominant part in the neutral mass matrix, also limits the WIMP mass[6]. If the general model is considered, the N/ω_0 composition in the WIMP defines, on grounds of above discussions, the strength of this constraint to the model parameters. Following the notation in [III] the maximum CM collision energy in LEP was $2\tilde{M} \approx 209$GeV. Thus the charged adjoint state needs to have mass $m_D^{\omega} > \tilde{M}$, which constrains the mixings through the relation $m_D^{\omega} \equiv |M_L^{\omega}| = |m_1 O_{21}^2 + \rho_{12} m_2 O_{22}^2 + \rho_{13} m_3 O_{23}^2| > \tilde{M}$. Of course this limit becomes tighter as $\tilde{M}$ increases in the course of LHC experiments. Another limit follows from requirement that the WIMP has to be lighter than the charged particle: $m_D^{\omega} > m_{\rm WIMP}$ ($m_{\rm WIMP}$ refers to the mass of lightest neutral mass eigenstate χ_i). These limits can severely constrain the general DM model.

4.6.2 Cryogenic limits

The direct DM-detection is searched in several cryogenic dark matter experiments. In these experiments using low temperature detectors a signal of the low recoil energy deposited by the WIMP to nuclide of the detector material in a soft elastic collisions[7] are searched. The most efficient experiments at the moment are the XENON100 [77] and the CDMSII [78] experiments and they give the most reliable[8] constrains to the WIMP-nucleon cross sections.

Constraining the DM model via cryogenic experiments is a highly non-trivial task, when several aspects related to the detector, the nuclides used, the WIMP-nucleon couplings and dark matter velocity and density distributions in the galactic neighborhood need to be considered[9]. The plausibility of given DM

[6] An accurate description of how to make this constraint for the 2×2 $\omega_0 - \beta$ mixture is given in [III] in Sec. III.A.

[7] Also inelastic collisions are studied, but these are not considered here.

[8] The recent XENON100 results [77] have rised a discussion [79, 80] of the positive DM signal in DAMA [81] and speculative signals seen in CDMSII [78] and CoGeNT [82]. For now the XENON100 results appear to be most the reliable. Yet there is a recent N-body simulation work [83], which might give some more consensus between the results of these different experiments.

[9] A general procedure how to take account of all of these aspects is given for example in

model is tested by calculating the expected collision count rate in a DM detector and then comparing it to the observed counts. No fully confirmed signal has been observed however[10], and therefore the observations have provided only limits on the model parameters and therein such as cross section.

To compare the results from different experiments it is most practical to invert the cross sections from the detector-specific WIMP-nuclide cross sections to the generic WIMP-nucleon cross sections. Of course to do this the nuclear structure information, implemented to the nuclear form factors, need to be known accurately. To make the cross section comparisons more convenient, the energy dependent form factors at the zero momentum transfer limit are usually employed.

Further, depending on the Dirac or Majorana nature of the DM particle the WIMP-nucleon interactions may in general proceed through a vector, an axial vector, a scalar and/or a pseudoscalar coupling. Since in the present case WIMPs are Majorana particles, only the Majorana couplings are considered here and thus the vector couplings are excluded. Further, in the non-relativistic limit, which is the case for WIMP-nucleon interactions assuming the usual WIMP masses and velocity distribution, the axial vector and the scalar couplings dominate over the pseudoscalar coupling. In the present case the WIMP can have an axial vector coupling to the Z-boson and a scalar coupling to the Higgs boson. Further, the axial vector current couples to the spin of the nucleus so that a WIMP-nucleon interaction which proceeds via Z-boson exchange through a axial vector current causes a spin-flip in the nucleus. This is called the *spin-dependent* WIMP-nucleon interaction. The WIMP-nucleon interaction via Higgs boson exchange is scalar and it does not affect the spin of the nucleus. This interaction is called a *spin-independent* WIMP-nucleon interaction. In the spin-dependent interaction case the WIMP only sees the unpaired valence nucleons in the nucleus which in general determine the nuclear spin. Thus only the nuclides with odd number of nucleons (neutron odd or proton odd depending on the nucleus) are sensitive to the spin-dependent interactions. Further, because of the weak isospin, the Z-boson couplings to neutrons and to protons are different and thus in the spin-dependent case the WIMP-nucleon coupling is usually specified to be either a pure WIMP-neutron coupling or a pure WIMP-proton coupling. Naturally both cases count but usually, depending on whether the nucleus is neutron odd or proton odd, one or the other is dominating. In the spin-independent interactions the WIMP sees the entire nucleus coherently. All nuclides are sensitive for the spin-independent interactions however, and no specification between the neutron/proton interaction is needed in this case. Since the physical nuclear final states are different for the spin-dependent and for the spin-independent interactions the corresponding interaction matrix elements cannot be coherently summed and the interaction channels need to be treated separately. For a typical WIMPs both interaction channels are possible but one usually dominates

article [II] Sec. 4.2.

[10]Besides the speculative DAMA [81], CDMSII [78] and CoGeNT [82] signals.

over the other. Still, in an accurate analysis both channels should be considered.

The spin-dependent WIMP-nucleon cross section[11] in zero momentum transfer limit is given by

$$\sigma^0_{\rm SD} = (O_{1i})^4 \frac{8G_F^2}{\pi} \mu^2_{\rm nuc} [a_p \langle S_p \rangle + a_n \langle S_n \rangle]^2 \frac{J+1}{J} \,, \tag{4.45}$$

where $\mu_{\rm nuc}$ is the WIMP nucleon reduced mass, $a_{p,n}$ and $\langle S_{p,n} \rangle$ are the nucleon spin factors[12] and spin expectation values for protons and neutrons respectively and the J is the total angular momentum of the nucleon. In calculations the EMC measurement values [84] for the WIMP nucleon spin factors are used which for pure proton (neutron) case is $a_p^2 = 0.46$ ($a_n^2 = 0.34$). Correspondingly the spin expectation values are $\langle S_p \rangle = 0.5$ and $\langle S_n \rangle = 0$ ($\langle S_n \rangle = 0.5$ and $\langle S_p \rangle = 0$). Finally $J = 1/2$ for both cases. For each value of $m_{\rm WIMP} \equiv m_i$, where i refers to the lightest state among the three neutral states, the mixing angle dependent O_{1i} factor, defined in equation (4.23) with (4.22), is chosen to give the correct dark matter density parameter value $\Omega_{\chi_{\rm WIMP}}(m_i, \vartheta_{ij}, \rho_{ij}) = 0.214$.

The spin-independent WIMP-nucleon cross section, again in zero momentum transfer limit, is

$$\sigma^0_{\rm SI} = (C^h_{ii})^2 \frac{8G_F^2}{\pi} \frac{m_i^2 m^2_{\rm nuc}}{m_H^4} K^2 \mu^2_{\rm nuc} \,, \tag{4.46}$$

where $m_{\rm nuc}$ is nucleon mass, m_H is the Higgs boson mass and the mass scenario and ρ_{ij}-phase and mixing angle dependent C^h_{ii}-factor is given in Table (4.1). The quantity $K \equiv (1/m_{\rm nuc}) \sum_q \langle {\rm nuc}|{\rm m_q}\bar{\rm q}{\rm q}|{\rm nuc}\rangle \approx 1/3$ is the normalized total scalar quark current within the nucleon. The sum in the K accounts for the fact that the WIMP can couple via Higgs to all quarks (valence and sea) within the nucleon. For the individual currents $\langle {\rm nuc}|{\rm m_q}\bar{\rm q}{\rm q}|{\rm nuc}\rangle$ the values given in ref. [85] is used. Also in this case the mixing angles are always chosen to produce the favorable cosmological dark matter density $\Omega_{\chi_{\rm WIMP}}(m_i, \vartheta_{ij}, \rho_{ij}) = 0.214$.

4.6.3 Other indirect limits

Dark matter may be expected to accumulate for example in the cores of the Sun and the Earth or in the center of the Galaxy and start to annihilate there. Thus indirect evidence of the dark matter can be searched via their annihilation end products such as diffuse gamma rays, charged particles and neutrinos. The accumulation process and the spectrum of the annihilation products are highly model dependent and an accurate evaluation of these is not discussed here. Still,

[11] Cross sections presented in Eqs. (4.45) and (4.46) are similar to those presented in [II] and [52]. However, the mixing angle dependent front factors are here of course more general.

[12] These are the effective WIMP-nucleon couplings which are dependent on the quark spin distribution within the nucleons and the nature of the WIMP (in present case the SM-like Majorana neutrino is considered).

even lacking the proper treatment of the accumulation and annihilation products for the model, the results from the indirect dark matter search experiments from the SuperKamiokande [86] and the IceCube [87] neutrino detectors can be inverted to limit the spin-dependent and spin-independent WIMP-nucleon cross sections. Using the model cross sections shown in Eqs. (4.45) and (4.46) the model mass parameter space can be constrained using these limits. Such bounds were established for the 2×2 doublet and 2×2 adjoint mixing models in articles [II] and [III] respectively. Based on these analyses, it was concluded that the complete IceCube detector, with the DeepCore extension installed, should be able to verify or severely constrain the most general DM model. Performing the analysis of these constraints in the most precise way possible, is one of the main aims in the future.

4.6.4 Oblique constrains

The polarization amplitudes of the EW gauge boson, which are most conveniently characterized with the oblique parameters S,T and U, as already discussed in the TC chapter, are affected by the new fermions coupled to the weak or electromagnetic interactions. Thus the new heavy particles; new leptons and SU(2) adjoint states present in the studied most general model, contribute to the S, T and U parameters whose values are highly constrained with the EW precision data from LEPII. This data can be used to constrain the masses and the mixings of the new particles. A general precision analysis for the most general 3×3 mixing DM model is still lacking, but the partial 2×2 doublet mixing model has been tested under the EW data in the article [II] (also the EW tests within the adjoint mixing model have been discussed in the article [III]). Suitable parameter space, consistent also with the precision data, for this model exists. The oblique parameter limits mainly constrain the mass ratio of the WIMP N and the charged state E in the doublet model. The general model will be tested under the EW data in upcoming article and at this point, based on the partial model consistency with the data, the acceptable parameter space for general model is also expected to exist.

Chapter 5

Summary and outlook

Several lines of evidence support the existence of the dark matter in the Universe. In the light of the present observations the particle dark matter, and in particular the WIMP scenario is a very promising alternative to solve the dark matter problem. In this context recent minimal walking techicolor model motivated dark matter models have been studied. The minimal walking techinicolor and the minimal extension of it, which can successfully provide a dynamical origin for the electroweak symmetry breaking as well as the unification of the standard model coupling constants, gives rise to natural dark matter candidates such as fourth family heavy neutrinos and SU(2) adjoint matter. A general model which combines these two dark matter scenarios has been considered here and numerical results and predictions in certain limits have been discussed. In general these models can produce the right amount of dark matter and the dark matter particles are within the reach of upcoming experiments. Thus, if existing, they may be detected in near future. One important side result in this thesis considers the effects of the Majorana phases of mixing particles to the model parameter space. Because of these phases, which are related to the mass eigenvalue positivity of the mixing Majorana states, the general physical parameter space of the model is larger than what usually has been thought.

Future studies include a complete Monte Carlo analysis of the parameter space, including all experimental constrains, of the most general 3×3 mixing dark matter model introduced in this thesis. Also a formulation of the general Feynman rules for the mixing Majorana particles is one of the immediate research goals.

Appendix

Here an explicit example for calculating the annihilation matrix element including mixing Majorana fields is given. The process considered is $\bar{\chi_3}\chi_3 \to ZZ$ of which only the χ_3-propagator part is demonstrated. This channel includes eight different initial state contractions following from the four different internal χ_3-contractions i.e. propagators. There are also two final state contractions so that altogether 16 contractions for this combined t/u-channel graph. Below is represented four of these contractions, one with each different propagator, and the first two and last two have different final state contractions. To help manipulations of the matrix elements a new notation in which the Dirac matrix indices are shown explicitly is adopted. In this notation the useful relations $\chi_i^c = C\bar{\chi}_i{}^T = \rho_i\chi_i$ and $\bar{\chi_i^c} = -\chi_i^T C^{-1}$ are denoted in matrix component form by; $\chi_\alpha^c = C_{\alpha\beta}\bar{\chi}^{T\beta} = C_{\alpha\beta}\bar{\chi}^\beta$ and $\bar{\chi}^{c\beta} = -\chi_\alpha^T C^{\alpha\beta} = -\chi_\alpha C^{\alpha\beta}$, where the charge conjugation matrices in component form are defined by; $C \cong C_{\alpha\beta}$ and $C^{-1} \cong C^{\alpha\beta}$ ($C^{-1} = C^\dagger = C^T = -C$). The matrix element is

$$\begin{aligned}
\mathcal{M}_{ZZ} \;=\; & A_{13}\big[\langle a_Z(k_2)a_Z(k_1)|(\bar{\chi}_3^\alpha[\not{Z}P_L]_\alpha{}^\sigma\chi_{3\sigma})_x(\bar{\chi}_3^\gamma[\not{Z}P_L]_\gamma{}^\beta\chi_{3\beta})_y|a^\dagger(p_2)a^\dagger(p_1)\rangle \\
& +\langle a_Z(k_2)a_Z(k_1)|(\bar{\chi}_3^\alpha[\not{Z}P_L]_\alpha{}^\sigma\chi_{3\sigma})_x(\bar{\chi}_3^\gamma[\not{Z}P_L]_\gamma{}^\beta\chi_{3\beta})_y|a^\dagger(p_2)a^\dagger(p_1)\rangle \\
& +\langle a_Z(k_2)a_Z(k_1)|(\bar{\chi}_3^\alpha[\not{Z}P_L]_\alpha{}^\sigma\chi_{3\sigma})_x(\bar{\chi}_3^\gamma[\not{Z}P_L]_\gamma{}^\beta\chi_{3\beta})_y|a^\dagger(p_2)a^\dagger(p_1)\rangle \\
& +\langle a_Z(k_2)a_Z(k_1)|(\bar{\chi}_3^\alpha[\not{Z}P_L]_\alpha{}^\sigma\chi_{3\sigma})_x(\bar{\chi}_3^\gamma[\not{Z}P_L]_\gamma{}^\beta\chi_{3\beta})_y|a^\dagger(p_2)a^\dagger(p_1)\rangle \\
& +12 \text{ other contractions}\big]
\end{aligned} \tag{5.1}$$

where $A_{13} \equiv \frac{i^2}{2}\left(\frac{g}{2\cos\theta_W}\right)^2(O_{13})^4$ with O_{ij} being the elements of the matrix U_D defined in Eq. (4.22) without the complex phase factors. Using the relations from Eq. (4.34) and Eq. (4.35) ($\rho_i^* = \rho_i$ here), and a careful bookkeeping of the

momentum factors in the propagators, the matrix element becomes:

$$\begin{aligned}\mathcal{M}_{ZZ} &= A_{13}\big[\rho_3\bar{v}(p_1)^\alpha(\not{Z}(k_1)P_L)_\alpha{}^\sigma(S(p_2-k_2))_\sigma{}^\gamma(\not{Z}(k_2)P_L)_\gamma{}^\beta u(p_2)_\beta \\ &\quad -\rho_3\bar{v}(p_1)^\gamma(\not{Z}(k_2)P_L)_\gamma{}^\beta(-C^{-1}S(p_1-k_2)C)^\alpha{}_\beta(\not{Z}(k_1)P_L)_\alpha{}^\sigma u(p_2)_\sigma \\ &\quad +\rho_3\bar{u}(p_2)_\sigma(\not{Z}(k_2)P_L)_\alpha{}^\sigma(\rho_3 C^{-1}S(p_1-k_1))^{\alpha\gamma}(\not{Z}(k_1)P_L)_\gamma{}^\beta u(p_1)_\beta \\ &\quad +\rho_3\bar{v}(p_2)^\alpha(\not{Z}(k_2)P_L)_\alpha{}^\sigma(-\rho_3 S(p_1-k_1)C)_{\sigma\beta}(\not{Z}(k_1)P_L)_\gamma{}^\beta\bar{v}(p_1)^\gamma \\ &\quad +12\text{ other terms}\big] \end{aligned} \tag{5.2}$$

where $S(q)$ is the usual Dirac propagator. To simplify the matrix elements further, the following relations become handy: $u_\alpha = C_{\alpha\beta}\bar{v}^{T\beta} = C_{\alpha\beta}\bar{v}^\beta$, $v_\alpha = C_{\alpha\beta}\bar{u}^{T\beta} = C_{\alpha\beta}\bar{u}^\beta$, $\bar{v}^\alpha = C^{\alpha\beta}u_\beta$ and $\bar{u}^\alpha = C^{\alpha\beta}v_\beta$. For a generic operator $\mathcal{O}$ it holds that $\bar{v}(p_a)\mathcal{O}u(p_b) = -\bar{v}(p_b)C\mathcal{O}^TC^{-1}u(p_a)$, and $C\gamma^{\mu T}C^{-1} = -\gamma^\mu$, $C\gamma^{5T}C^{-1} = \gamma^5$. Propagators are easily manipulated in component form, e.g. $(-C^{-1}S(q)C)^\alpha{}_\beta = -C^{\alpha\gamma}S(q)_\gamma{}^\sigma C_{\sigma\beta} = -C_{\beta\sigma}S^T(q)^\sigma{}_\gamma C^{\gamma\alpha} = -(CS^T(q)C^{-1})_\beta{}^\alpha = -S(-q)_\beta{}^\alpha$. After manipulating all the 16 terms in this way, the matrix element finally reduces to:

$$\begin{aligned}\mathcal{M}_{ZZ} &= i\left(\tfrac{g}{2\cos\theta_W}\right)^2\rho_3(O_{13})^4\epsilon_\mu^Z(k_1)\epsilon_\nu^Z(k_2)\times \\ &\quad \bar{v}(p_1)\big[D_3^t\gamma^\mu(\not{p}_1-\not{k}_1+m_3)\gamma^\nu + D_3^u\gamma^\nu(\not{p}_1-\not{k}_2+m_3)\gamma^\mu\big]u(p_2)\end{aligned} \tag{5.3}$$

where propagator $D_3^j \equiv 1/(j-m_3^2)$. One should notice that the total $\bar{\chi_3}\chi_3 \to ZZ$ matrix element, which is not represented here, includes also the t- and u-channel graphs with χ_1-and χ_2-propagators and also s-channel with Higgs propagator. In these channels also the phase factors ρ_i will have more transparent role as they explicitly exist in the interaction vertices, as seen from the Eq. (4.29) and Eq. (4.32).

References

[I] K. Kainulainen, K. Tuominen and J. Virkajarvi, "Weakly interacting dark matter particle of a minimal technicolor theory," Phys. Rev. D **75** (2007) 085003 [arXiv:hep-ph/0612247].

[II] K. Kainulainen, K. Tuominen and J. Virkajarvi, "Weakly interacting dark matter from the minimal walking technicolor," JCAP **1002** (2010) 029 [arXiv:0912.2295 [astro-ph.CO]].

[III] K. Kainulainen, K. Tuominen and J. Virkajarvi, "Naturality, unification and dark matter," Phys. Rev. D **82** (2010) 043511, [arXiv:1001.4936].

[1] M. Colless *et al.* [The 2dF galaxy redshift survey], http://www.mso.anu.edu.au/2dFGRS/; M. Colless, "First results from the 2dF galaxy redshift survey," arXiv:astro-ph/9804079.

[2] B. J. Boyle *et al.* [The 2dF QSO redshift survey], http://www.2dfquasar.org/; T. Shanks, B. J. Boyle, S. M. Croom, N. Loaring, L. Miller and R. J. Smith, "2dF QSO Redshift Survey," arXiv:astro-ph/0003206.

[3] C. L. Bennett *et al.* [WMAP Collaboration], "First Year Wilkinson Microwave Anisotropy Probe (WMAP) Observations: Preliminary Maps and Basic Results," Astrophys. J. Suppl. **148** (2003) 1 [arXiv:astro-ph/0302207]; NASA LAMBDA-projects [COBE and WMAP collaborations] http://lambda.gsfc.nasa.gov/

[4] [Particle Data Group], http://pdg.lbl.gov/2009/reviews/contents_sports.html

[5] V. Mukhanov, "Physical Foundations of Cosmology," Cambridge University Press (2005)

[6] H. Ohanian and R. Ruffini "Gravitation and Spacetime," second edition, W.W. Norton & Company (1994)

[7] S. Tsujikawa, "Introductory review of cosmic inflation," arXiv:hep-ph/0304257.

[8] N. Jarosik *et al.*, "Seven-Year Wilkinson Microwave Anisotropy Probe (WMAP) Observations: Sky Maps, Systematic Errors, and Basic Results," arXiv:1001.4744 [astro-ph.CO].

[9] B. Fields and S. Sarkar, "Big-bang nucleosynthesis (PDG mini-review)," arXiv:astro-ph/0601514.

[10] M. S. Turner and D. Huterer, "Cosmic Acceleration, Dark Energy and Fundamental Physics," J. Phys. Soc. Jap. **76** (2007) 111015 [arXiv:0706.2186 [astro-ph]].

[11] T. Mattsson, *Dark energy as a mirage*, arXiv:0711.4264 [astro-ph], Gen. Relativ. Gravit. [doi:10.1007/s10714-009-0873-z]

[12] K. Kainulainen and D. Sunhede, "On the stability of spherically symmetric spacetimes in metric f(R) gravity," Phys. Rev. D **78** (2008) 063511 [arXiv:0803.0867 [gr-qc]].

[13] P. J. E. Peebles and B. Ratra, "Cosmology with a time variable cosmological "constant"," Astrophys. J. **325** (1988) L17; B. Ratra and P. J. E. Peebles, "Cosmological consequences of a rolling homogeneous scalar field," Phys. Rev. D **37** (1988) 3406;

[14] M. Joyce, "On the expansion rate of the universe at the electroweak scale," Phys. Rev. D **55**, 1875 (1997) [arXiv:hep-ph/9606223].

[15] J. H. Oort, "The force exerted by the stellar system in the direction perpendicular to the galactic plane and some related problems", Bull. Astron. Inst. Netherlands, **6**, 249 (1932)

[16] Zwicky F., 1933, Helvetica Physica Acta 6 110

[17] M. Kamionkowski, "Possible relics from new physics in the early universe: Inflation, the cosmic microwave background, and particle dark matter," arXiv:astro-ph/9809214.

[18] J. Binney and S. Tremaine "Galactic Dynamics," Princeton University Press (2005)

[19] M. Roos, "Dark Matter: The evidence from astronomy, astrophysics and cosmology," arXiv:1001.0316 [astro-ph.CO].

[20] M. Persic and P. Salucci, "The baryon content of the Universe," arXiv:astro-ph/0502178.

[21] A. Petric, G. A. Telis, F. Paerels and D. J. Helfand, "A Direct Upper Limit on the Density of Cosmological Dust from the Absence of an X-ray Scattering Halo around the z=4.3 QSO 1508+5714," Astrophys. J. **651** (2006) 41 [arXiv:astro-ph/0609589].

[22] C. Alcock *et al.* [MACHO Collaboration], "The MACHO project: Microlensing results from 5.7 years of LMC observations," Astrophys. J. **542** (2000) 281 [arXiv:astro-ph/0001272].

[23] P. Tisserand *et al.* [EROS-2 Collaboration], "Limits on the Macho Content of the Galactic Halo from the EROS-2 Survey of the Magellanic Clouds," Astron. Astrophys. **469** (2007) 387 [arXiv:astro-ph/0607207].

[24] J. Yoo, J. Chaname and A. Gould, "The End of the MACHO Era: Limits on Halo Dark Matter from Stellar Halo Wide Binaries," Astrophys. J. **601** (2004) 311 [arXiv:astro-ph/0307437].

[25] B. Carr, K. Kohri, Y. Sendouda and J. Yokoyama, "New cosmological constraints on primordial black holes," arXiv:0912.5297 [astro-ph.CO].

[26] B. C. Lacki and J. F. Beacom, "Primordial Black Holes as Dark Matter: All or Nothing," arXiv:1003.3466 [astro-ph.CO].

[27] S. Hannestad, "The connection between cosmology and neutrino physics," arXiv:1003.4119 [astro-ph.CO].

[28] J. E. Kim and G. Carosi, "Axions and the Strong CP Problem," arXiv:0807.3125 [hep-ph].

[29] S. Hannestad, A. Mirizzi, G. G. Raffelt and Y. Y. Y. Wong, "Neutrino and axion hot dark matter bounds after WMAP-7," arXiv:1004.0695 [astro-ph.CO].

[30] M. Milgrom, "A Modification Of The Newtonian Dynamics As A Possible Alternative To The Hidden Mass Hypothesis," Astrophys. J. **270** (1983) 365.

[31] J. D. Bekenstein, "Relativistic MOND as an alternative to the dark matter paradigm," Nucl. Phys. A **827** (2009) 555C [arXiv:0901.1524 [astro-ph]].

[32] A. Knebe, "MONDian Cosmological Simulations," arXiv:astro-ph/0509665.

[33] C. Llinares, A. Knebe and H. Zhao, "Cosmological Structure Formation under MOND: a new numerical solver for Poisson's equation," arXiv:0809.2899 [astro-ph].

[34] R. Massey, T. Kitching and J. Richard, "The dark matter of gravitational lensing," arXiv:1001.1739 [astro-ph.CO].

[35] L. Fu *et al.*, "Very weak lensing in the CFHTLS Wide: Cosmology from cosmic shear in the linear regime," Astron. Astrophys. **479** (2008) 9 [arXiv:0712.0884 [astro-ph]].

[36] D. Clowe, M. Bradac, A. H. Gonzalez, M. Markevitch, S. W. Randall, C. Jones and D. Zaritsky, "A direct empirical proof of the existence of dark matter," Astrophys. J. **648** (2006) L109 [arXiv:astro-ph/0608407].

[37] J. R. Brownstein and J. W. Moffat, "The Bullet Cluster 1E0657-558 evidence shows Modified Gravity in the absence of Dark Matter," Mon. Not. Roy. Astron. Soc. **382** (2007) 29 [arXiv:astro-ph/0702146].

[38] K. Enqvist, K. Kainulainen and J. Maalampi, "Cosmic abundances of very heavy neutrinos," Nucl. Phys. B **317** (1989) 647.

[39] K. Enqvist, K. Kainulainen and J. Maalampi, "Singlet neutrinos in cosmology," Nucl. Phys. B **316** (1989) 456.

[40] R. Foadi, M. T. Frandsen and F. Sannino, *Technicolor Dark Matter,* Phys. Rev. D **80**, 037702 (2009) [arXiv:0812.3406 [hep-ph]].

[41] S. B. Gudnason, C. Kouvaris and F. Sannino, *Dark Matter from new Technicolor Theories*, Phys. Rev. D **74**, 095008 (2006) [arXiv:hep-ph/0608055];

[42] S. B. Gudnason, C. Kouvaris and F. Sannino, *Towards working technicolor: Effective theories and dark matter*, Phys. Rev. D **73**, 115003 (2006) [arXiv:hep-ph/0603014].

[43] C. Kouvaris, "Dark Majorana from the minimal walking technicolor," arXiv:hep-ph/0703266.

[44] K. Enqvist and K. Kainulainen, "Limits on heavy WIMP masses and interactions," Phys. Lett. B **264**, 367 (1991).

[45] J. Bernstein, "Kinetic theory in the expanding universe," Cambridge university press (1988).

[46] E. W. Kolb and M. S. Turner " The Early Universe", Perseus Books 1990 (paperback edition 1994).

[47] J. Bernstein, L. Brown and G. Feinberg *Cosmological heavy-neutrino problem*, Phys. Rev. D **32**, 3261 (1985).

[48] B. W. Lee and S. Weinberg, "Cosmological lower bound on heavy-neutrino masses," Phys. Rev. Lett. **39** (1977) 165.

[49] P. Salati, "Quintessence and the Relic Density of Neutralinos," Phys. Lett. B **571** (2003) 121 [arXiv:astro-ph/0207396].

[50] R. Catena, N. Fornengo, A. Masiero, M. Pietroni and F. Rosati, "Enhancement of dark matter abundance in scalar-tensor dark energy," arXiv:astro-ph/0406152; R. Catena, N. Fornengo, A. Masiero, M. Pietroni and F. Rosati, "Dark matter relic abundance and scalar-tensor dark energy," Phys. Rev. D **70** (2004) 063519 [arXiv:astro-ph/0403614].

[51] R. Catena and P. Ullio, "A novel determination of the local dark matter density," arXiv:0907.0018 [astro-ph.CO].

[52] J. Angle *et al.*, *Limits on spin-dependent WIMP-nucleon cross-sections from the XENON10 experiment*, Phys. Rev. Lett. **101** (2008) 091301 [arXiv:0805.2939 [astro-ph]].

[53] P. Gondolo and G. Gelmini, "Cosmic abundances of stable particles: Improved analysis," Nucl. Phys. B **360**, 145 (1991).

[54] C. T. Hill and E. H. Simmons, "Strong dynamics and electroweak symmetry breaking," Phys. Rept. **381** (2003) 235 [Erratum-ibid. **390** (2004) 553] [arXiv:hep-ph/0203079].

[55] F. Sannino, "Conformal Dynamics for TeV Physics and Cosmology," arXiv:0911.0931 [hep-ph].

[56] E. Farhi and L. Susskind, "A Technicolored G.U.T," Phys. Rev. D **20** (1979) 3404.

[57] T. Appelquist, M. Piai and R. Shrock, "Fermion masses and mixing in extended technicolor models," Phys. Rev. D **69** (2004) 015002 [arXiv:hep-ph/0308061].

[58] E. Eichten and K. D. Lane, Phys. Lett. B **90** (1980) 125.

[59] F. Sannino and K. Tuominen, "Techniorientifold," Phys. Rev. D **71** (2005) 051901 [arXiv:hep-ph/0405209].

[60] E. Witten, "An SU(2) anomaly," Phys. Lett. B **117** (1982) 324.

[61] A. J. Hietanen, K. Rummukainen and K. Tuominen, "Evolution of the coupling constant in SU(2) lattice gauge theory with two adjoint fermions," Phys. Rev. D **80** (2009) 094504 [arXiv:0904.0864 [hep-lat]].

[62] D. D. Dietrich, F. Sannino and K. Tuominen, "Light composite Higgs from higher representations versus electroweak precision measurements: Predictions for LHC," Phys. Rev. D **72** (2005) 055001 [arXiv:hep-ph/0505059].

[63] D. D. Dietrich, F. Sannino and K. Tuominen, "Light composite Higgs and precision electroweak measurements on the Z resonance: An update," Phys. Rev. D **73** (2006) 037701 [arXiv:hep-ph/0510217].

[64] R. Foadi, M. T. Frandsen, T. A. Ryttov and F. Sannino, "Minimal Walking Technicolor: Set Up for Collider Physics," Phys. Rev. D **76** (2007) 055005 [arXiv:0706.1696 [hep-ph]].

[65] E. H. Simmons, *Phenomenology of a Technicolor Model with Heavy Scalar Doublet*, Nucl. Phys. B **312**, 253 (1989).

[66] M. Antola, M. Heikinheimo, F. Sannino and K. Tuominen, "Unnatural Origin of Fermion Masses for Technicolor," JHEP **1003** (2010) 050 [arXiv:0910.3681 [hep-ph]].

[67] O. Antipin, M. Heikinheimo and K. Tuominen, "Natural fourth generation of leptons," JHEP **0910** (2009) 018 [arXiv:0905.0622 [hep-ph]].

[68] S. B. Gudnason, T. A. Ryttov and F. Sannino, "Gauge coupling unification via a novel technicolor model," Phys. Rev. D **76** (2007) 015005 [arXiv:hep-ph/0612230].

[69] D. D. Dietrich and F. Sannino, "Walking in the SU(N)," Phys. Rev. D **75** (2007) 085018 [arXiv:hep-ph/0611341].

[70] L. F. Li and F. Wu, *Coupling constant unification in extensions of standard model*, Int. J. Mod. Phys. A **19**, 3217 (2004) [arXiv:hep-ph/0304238].

[71] B. Bajc, M. Nemevsek and G. Senjanovic, *Probing seesaw at LHC*, Phys. Rev. D **76**, 055011 (2007) [arXiv:hep-ph/0703080].

[72] C. Giunti and C.W. Kim, "Fundamentals of Neutrino Physics and Astrophysics," Chapters 3,4,6, Oxford University Press (2007).

[73] J. R. Ellis, D. V. Nanopoulos, L. Roszkowski and D. N. Schramm, Phys. Lett. B **245**, 251 (1990)

[74] S. Eidelman *et al.* [Particle Data Group], "Review of particle physics," Phys. Lett. B **592**, 1 (2004).

[75] G. Jungman, M. Kamionkowski and K. Griest, *Supersymmetric dark matter*, Phys. Rept. **267** (1996) 195 [arXiv:hep-ph/9506380].

[76] E. Aprile, L. Baudis and f. t. X. Collaboration, "Status and Sensitivity Projections for the XENON100 Dark Matter Experiment," arXiv:0902.4253 [astro-ph.IM].

[77] E. Aprile *et al.* [XENON100 Collaboration], "First Dark Matter Results from the XENON100 Experiment," arXiv:1005.0380 [astro-ph.CO].

[78] Z. Ahmed *et al.* [The CDMS-II Collaboration and CDMS-II Collaboration], *Results from the Final Exposure of the CDMS II Experiment*, arXiv:0912.3592 [astro-ph.CO].

[79] J. I. Collar and D. N. McKinsey, "Comments on 'First Dark Matter Results from the XENON100 Experiment'," arXiv:1005.0838 [astro-ph.CO].

[80] T. X. Collaboration, "Reply to the Comments on the XENON100 First Dark Matter Results," arXiv:1005.2615 [astro-ph.CO].

[81] R. Bernabei *et al.* [DAMA Collaboration], "First results from DAMA/LIBRA and the combined results with DAMA/NaI," Eur. Phys. J. C **56** (2008) 333 [arXiv:0804.2741 [astro-ph]].

[82] C. E. Aalseth *et al.* [CoGeNT collaboration], "Results from a Search for Light-Mass Dark Matter with a P-type Point Contact Germanium Detector," arXiv:1002.4703 [astro-ph.CO].

[83] F. S. Ling, E. Nezri, E. Athanassoula and R. Teyssier, "Dark Matter Direct Detection Signals inferred from a Cosmological N-body Simulation with Baryons," JCAP **1002** (2010) 012 [arXiv:0909.2028 [astro-ph.GA]].

[84] J. R. Ellis and M. Karliner, "Determination of alpha s and the nucleon spin decomposition using recent polarized structure function data," Phys. Lett. B **341** (1995) 397 [arXiv:hep-ph/9407287].

[85] P. Gondolo, *Phenomenological introduction to direct dark matter detection*, arXiv:hep-ph/9605290.

[86] S. Desai *et al.* [Super-Kamiokande Collaboration], *Search for dark matter WIMPs using upward through-going muons in Super-Kamiokande*, Phys. Rev. D **70**, 083523 (2004) [Erratum-ibid. D **70**, 109901 (2004)] [arXiv:hep-ex/0404025].

[87] R. Abbasi *et al.* [ICECUBE Collaboration], *Limits on a muon flux from neutralino annihilations in the Sun with the IceCube 22-string detector*, Phys. Rev. Lett. **102** (2009) 201302 [arXiv:0902.2460 [astro-ph.CO]].

Paper I

Weakly interacting dark matter particle of a minimal technicolor theory
K. Kainulainen, K. Tuominen and J. Virkajarvi,
Phys. Rev. D **75** (2007) 085003 [arXiv:hep-ph/0612247].

Paper II

Weakly interacting dark matter from the minimal walking technicolor
K. Kainulainen, K. Tuominen and J. Virkajarvi,
JCAP **1002** (2010) 029 [arXiv:0912.2295 [astro-ph.CO]].

Paper III

Naturality, unification and dark matter,
K. Kainulainen, K. Tuominen and J. Virkajarvi,
Phys. Rev. D **82** (2010) 043511, [arXiv:1001.4936].